TRIBHUVAN UNIVERSITY

INSTITUTE OF ENGINEERING

PULCHOWK CAMPUS

A Report on

Design, Numerical Modelling and Performance Analysis of Vertical Axis Helical Wind Turbine: A Case Study at Sallaghari

By

Pradeep Bartaula

A REPORT

SUBMITTED TO THE DEPARTMENT OF MECHANICAL AND AEROSPACE ENGINEERING

IN PARTIAL FULFILLMENT OF THE REQUIREMENTS FOR

THE DEGREE OF MASTER IN

MECHANICAL SYSTEMS DEISGN AND ENGINEERING

DEPATRMENT OF MECHANICAL AND AEROSPACE ENGINEERING

LALITPUR, NEPAL

JULY,2020

COPYRIGHT

TRIBHUVAN UNIVERSITY

INSTITUTE OF ENGINEERING

PULCHOWK CAMPUS

DEPARTMENT OF MECHANICAL AND AEROSPACE ENGINEERING

The undersigned certify that they have read, and recommended to the Institute of Engineering for acceptance, a thesis entitled " **Design, Numerical Modelling and Performance Analysis of Vertical Axis Helical Wind Turbine: A Case Study at Sallaghari** " submitted by Pradeep Bartaula in partial fulfillment of the requirements for the degree of Master in Mechanical System Design and Engineering.

_____

Supervisor, Assoc. Prof. Dr. Shree Raj Shakya

Department of Mechanical and Aerospace Engineering,

Pulchowk Campus

_____

External Examiner, Dr. Ishwor Bajracharya

Nepal Academy of Science and Technology (NAST)

_____

Committee Chairperson, Dr. Nawraj Bhattarai

Head, Department of Mechanical and Aerospace

Engineering, Pulchowk Campus

Date: 30 July 2020

ABSTRACT

Wind energy is extremely vital in the development of sustainable energy with the growing focus on renewable energy. Interests in design of wind turbines has also been expanding. This research work is all about the design and numerical modelling of the vertical axis helical wind turbine for high power generation at Sallaghari. The rotor blades of varying aspect ratio were designed in CATIA V5R20 and simulation was carried out in ANSYS Workbench 18.1 and necessary data were obtained via computational fluid dynamic approach. Furthermore, the design was imported to rapid prototyping machine for fabrication of the rotor blade which later was assembled to proper frame arrangement and finally testing was carried out. The CFD approach was used for evaluation of highly efficient rotor with varying the aspect ratio and it has shown the turbine with aspect ratio of 1 to be the most efficient with performance coefficient of 0.3927. Under performance analysis section, both experimental and CFD data were used for numerical modelling validation. From the data obtained experimentally, the fabricated VAHWT has been found to operate at the low cut-in speed of 3.59 m/s and maximum power output has been found to be 7.76 watts at the wind speed of 11 m/s. The maximum rpm of the rotor blade was recorded to be 708.2 rpm at the velocity of 11.51 m/s signifying its potentiality of wind power production. At the end, the data obtained from both the process when analyzed through graph plots, had shown the similar nature slope wise. This simply signified the generation of satisfactory data via experiment. Moreover, the mechanical losses had shown difference between the experimental and data obtained via CFD approach. The 2-wheeled vehicles had the highest average speed than other mode of vehicles and the average speed of the vehicles among all modes was 57 Km/hr available at Sallaghari highway. The experimental data carried out at Sallaghari highway demonstrates that the maximum impact wind velocity of 7.86 m/s with 3.46 watts power generation, was available at 4 pm due to heavy duty vehicle and more traffic in highways. The average impact wind energy available at Sallaghari highway was 1.53 watts at the wind speed of 5.83 m/s. It can also be economical method of power extraction from wind in the country like Nepal with growing urbanisation.

ACKNOWLEDGEMENT

Last but not the least, I would like to pay my acknowledgement towards my family and friends for their continuous and unparalleled love, guidance and paving me a path to achieve this opportunity. Without their unconditional love and support, I would not have been able to achieve this today. I consider this opportunity as a massive milestone in my career development and looking forward to the future.

TABLE OF CONTENTS

LIST OF FIGURES

9

LIST OF TABLES

LIST OF ABBREVIATIONS

Particular	Description
ADC	Analog to Digital Converter
CFD	Computational Fluid Dynamics
CFRP	Carbon Fiber Reinforce Plastic
DC	Direct Current
DNA	De-oxy Ribonucleic Acid
FOS	Factor of Safety
GEC	Global Energy Council
GRP	Glass Reinforce Polyester
HAWT	Horizontal Axis Wind Turbine
IGES	Initial Graphics Exchange Specification
KE	Kinetic Energy
NEA	Nepal Electricity Authority
Rpm	Revolution per minute
RPM	Rapid Prototyping Machine
SST	Shear-Stress Transport
SWERA	Solar and Wind Energy Resource Assessment
SWMG	Solar Wind Mini Grid
VAHWT	Vertical Axis Helical Wind Turbine
VAWT	Vertical Axis Wind Turbine
VDC	Village Development Committee
WS	Windside

LIST OF SYMBOLS

Symbol	Description
A_s	Swept area of rotating blades
B	Aspect ratio
D	Diameter of rotor
d	Diameter of shaft
H	Height of rotor
I	Current
m	Mass of air transferring
N	Rotational speed of turbine
P	Power
R	Radius of rotor
T	Torque
T	Tensile strength of ABS plastic
v	Velocity of air
V	Voltage
λ	Tip speed ratio
ρ	Density of air

CHAPTER ONE: INTRODUCTION

1.1 Background

Nepal bestowed with 6000 rivers and rivulets with a technically feasible power production capacity of 42GW of electricity, is still not unable to generate sufficient energy to meet the demand (Pokharel, 2001). The need of electricity is increasing at an exponential rate. Considering the numbers, the annual peak power demand in the fiscal year 2018/19 was 1320.28 MW, out of which only 1182.225 MW capacity was installed (NEA, 2019). To overcome this gap, Nepal should find such resources that can be utilized even in the dry season so that there could be optimum production of energy to meet the needs. As Nepal fully relies on hydropower for electricity, the exploration of other resources has yet to be done and many studies show the immense possibilities to generate electricity from various other means such as solar and wind.

Considering wind power potential in Nepal, a study done jointly by the Department of Geology at Tribhuwan University and the Ministry of Physical Planning and Works found at least, 3,000 MW of technical wind potential and 448 MW of potential that could be quickly and commercially exploited. Not only that the other study also shows the estimated power generation utilizing wind resources in the Annapurna Conservation Area alone could extract at least 716 MW that is within 10 kilometers of the NEA grid. Since there is steep growth in demand of electricity, the utilization of wind power could help the nation to fill the gap between power production and demand. Besides this wind harvesting could be a very efficient method for rural electrification. Despite having this capacity, nation hasn't even extracted 1MW of power in total yet (Upreti & Shakya, 2009).

Nepal has installed only HAWT for wind power extraction, and VAWT is not being used. The use of a VAWT wind turbine can help in more power extraction at low speed and low altitude. Exploiting the wind resources available in the country using VAWT can be a boon in the energy sector helping the nation to supply energy as per its demand.

1.2 Wind Energy

 The uneven heating of the atmosphere, irregular earth's surface, and earth rotation are the major reasons for wind power generation. Recently two wind turbines each of 5 kW capacities with 40 kW of solar hybrid system has been implemented in Pamakham, Bhojpur district supported by Asian Development Bank. Most of the existing mini wind-solar hybrid projects were used for households proposed like lighting, mobile charging, router, TV etc. The first two horizontal axis wind turbine of each 5kW was installed at Nawalparasi with 2kW solar hybrid system. The total wind energy plant of 163kW capacity were installed in Nepal till 2019 with the solar hybrid system of 221kW capacity. The below table gives information about the existing horizontal axis wind turbine installation in various places in Nepal.

Table 1.1: Existing horizontal axis wind turbine installation in various places of Nepal (Rai, 2019)

| S.N. | Project Name | District | Installed Capacity Kw | | | Year of Installation |
			Solar PV Plant	Wind Turbines	Total	
1	Dhaubadi SWMG	Nawalparasi	2	10	12	2010
2	Bhorleni SWMG	Makawanpur	15	10	25	2013
3	Tatopani SWMG	Jumla	11	15	26	2014
4	Kamalbazar SWMG	Achham	11	20	31	2015
5	Harrekanda-Taranga SWMG	Surkhet	5	3	8	2015
6	Chisapani SWMG	Sindhuli	15	20	35	2016
7	Parakatne SWMG	Bajhang	7	15	22	2016
8	Mityal SWMG	Palpa	15	10	25	2017
9	Narakot SWMG	Jumla	50	30	80	2017
10	Saptami SWMG	Panchthar	50	20	70	2018
11	Pamakham SWMG	Bhojpur	40	10	50	2019
Total Capacity kW			**221**	**163**	**384**	

1.3 Wind Turbine

A wind turbine is a mechanical device that converts the kinetic energy to electrical energy. The wind turns the blades, the kinetic energy converted to the mechanical energy and the rotor is connected with the generator with the help of a shaft which can generate electrical energy with the help of the magnetic field available in the generator.
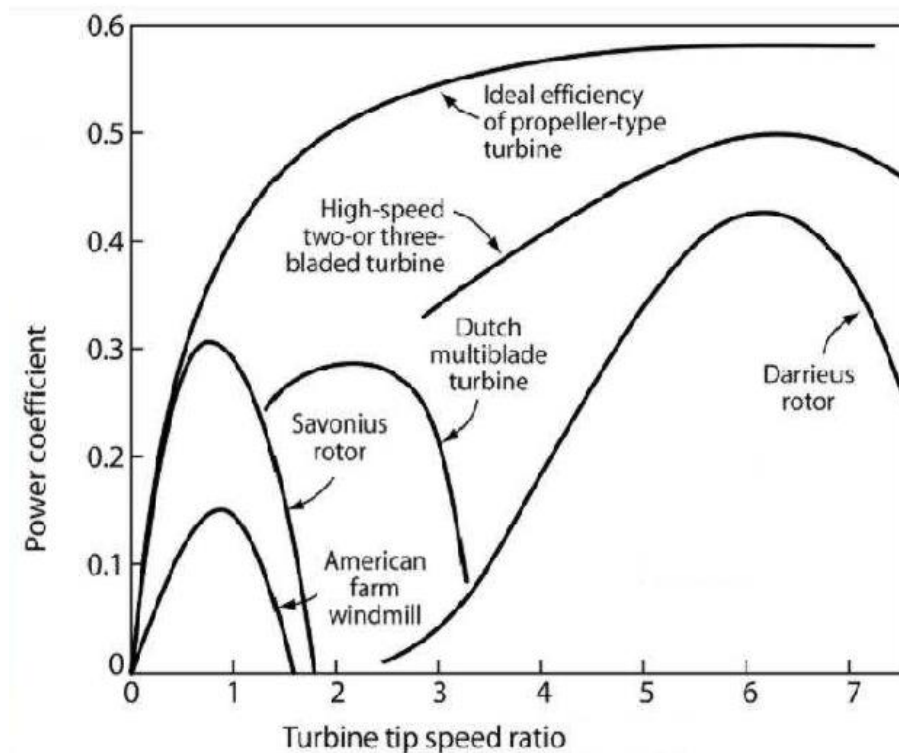
Figure 1.1: Power Coefficient vs Tip Speed Ratio for Various Wind Turbines

(Eldridge, 1975)

Wind turbines are categorized into two types on the basis of shaft mounted which are explain below:

a) **Vertical axis wind turbine (VAWT):** The wind turbine which has a shaft-mounted perpendicular to the ground, is known as a vertical axis wind turbine. It does not require any tailfin or yaw mechanism i.e. it catches the wind from all the directions.

b) **Horizontal axis wind turbine (HAWT):** The wind turbine which has a shaft mounted parallel to the ground, is known as a horizontal axis wind turbine. It requires the tailfin or yaw mechanism to determine the air direction for power generation throughout the day.

1.4 Helical Wind Turbines

Nowadays, vertical axis helical wind turbines have grown in popularity for urban and domestic use. The vertical axis helical wind turbines look like DNA structures or large drill bits. There are several advantages such as low noise level, less risk of bird injury, slower speed along the blade tip, less maintenance cost etc. make it more feasible for installation.

Advantage of vertical axis Helical wind turbine over horizontal axis wind turbine:

There are several advantages of vertical axis helical wind turbines over a horizontal axis wind turbine. These advantages are listed below.

a. They are installed at a low level from the ground which reduces the maintenance cost.
b. They generate electricity at low wind speed.
c. They have a low noise level i.e. environment friendly.
d. They have less risk of bird's injury due to lower speed along the blade tip.

1.5 Global Applications

The global new wind power installations surpassed by 60GW in 2019 i.e. 19 percentage growth compared to 2018 and bringing the total installed capacity to 650GW, a growth of 10 percent compared to last year.
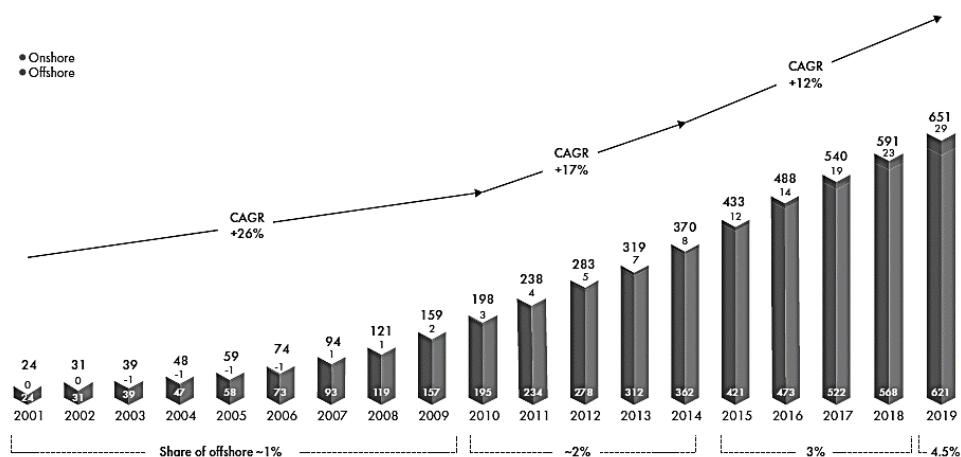
Figure 1.2: Global trend in wind energy (GW) *(GWEC, 2019)*

China, the US, United Kingdom, India, and Spain are the world's top five wind power installation countries in 2019 and they together contribute 70% of world wind power installation last year. The total wind power installation increased by 2% at the end of 2019.

1.6 Impact Wind on Highways

Impact wind energy is one of the wind energies created by the moving vehicles. When the vehicles are moving on highways, the creation of a pressure column occurred on both sides of the roads. Due to the difference between the pressure column, the flow of wind occurred which is known as impact wind. It is mainly depending on the size of the vehicles, frequency of the vehicles, speed of the vehicles etc.

1.7 Problem Statement

A major problem in the development of wind energy is fluctuation in the sources of wind. Highways appear to be a sufficient source of potential wind energy. However, there are very much few wind energy plants installed and all the plants are horizontal axis wind turbines. Therefore, there are very little researches conducted on the vertical axis helical wind turbine performance and there was no vertical axis wind turbine installed in Nepal till now. The highway is one of the rich sources of impact wind energy. Also, there was very less study conducted on highway impact wind energy assessment in Nepal. In this context, a study of vertical axis helical wind turbines and impact wind energy potential might shed light on the development of wind power generation on different highways for street light and traffic signals.

1.8 Objectives of Thesis

The main objective is to design, conduct numerical modeling and performance analysis of vertical axis helical wind turbines for the use of the maximum amount of wind energy from vehicles running on highways. The specific objectives are listed below:

a) To design and conduct numerical modeling of VAHWT with a variable aspect ratio
b) To fabricate the prototype with high-efficiency aspect ratio and evaluate the performance of VAHWT
c) To study the wind potential for VAHWT at Sallaghari.

1.9 Limitations

There were some limitations which are listed below:

- The effect of twist angle on the performance coefficient was not considered
- The error from different measurement instrument used was neglected
- Loss due to rough rotor surface was not accounted
- Face and edge meshing have been used under numerical modeling section

CHAPTER TWO: LITERATURE REVIEW

This research work is about the design, Numerical Modelling, and performance analysis of VAHWT, which mainly deals with the design and modeling of the Helix structured rotor profile. The numerous numbers of advantages over other forms of HAWT and VAWT has increased its popularity in the recent world. Still the current practice in the world shows very limited development in the field of Helix structured VAWT because of its complex blade design. Thus, the emphasis has been laid on the design of VAHWT and the performance evaluation of the Helix structured rotor.

The research was carried on the relation between aspect ratio and performance of the vertical axis wind turbine. The study found that the turbine with a lower aspect ratio had a higher power coefficient. An added advantage of greater in-service stability was observed due to structure by having a thicker blade (S. Brusca, et al., 2014).

A similar study was carried out by Md Aminul Hassan and Dr. C B Vijaya Vitala. The study was experimented to analyze the potential of energy extraction from the wind on highways. The study showed that the maximum potential of impact wind energy was available at a height of 120 cm from the ground level. The aspect ratio is one of the major criteria to be considered in the design of VAWT (Md & C B, 2014).

The experiment was done with a 20-degree twist helical wind turbine at different overlap conditions. Six different overlap ratios were taken for analysis and it was concluded that the maximum coefficient of performance of 0.289 was available at 12.76% overlap ratio. And the tip speed ratio of 0.5-0.9 was concluded as the best performance for the recommendation (Deb*, et al., 2014).

The research work presented about the effects of different types of end plates on the vertical axis helical wind turbine with a 180-degree twist. Four different endplates were taken for analysis and it was concluded that the blade with end plates on both top and bottom increased the performance coefficient by up to 36% than the model with no endplates (Keum, et al., 2015).

Arturo Reza and his friends developed a prototype of VAHWT which produced 1500 kW/h per year power at a velocity of 10.2 m/s with a swept area of 1 m^2 (Reza, et al., 2015).

A study was carried out on the Performance Analysis of a Helical Savonius Wind Turbine with Modified Rotor. The study found that the modified helical rotor with a twist is found to attain the highest Cp of 0.22, as compared to 0.174 for the conventional rotor, with a performance gain of 26.4% (Saad, et al., 2017).

Aerodynamic analysis of a helical vertical axis wind turbine was carried out. The result from this study was found that the maximum performance coefficient of 0.1 was available at 1.8 tip speed ratio and the maximum power fluctuation coefficient can reach up to 150% under lower tip speed ratio conditions (Qian, et al., 2017).

The similar study was done on the Savonius wind turbine and proposed a modification in its design. The proposed modification adds a plane in the center and due to the mechanical modification of the rotor, the power coefficient was shown to be increased by around 8 percent (Svetlana, 2016).

A study was done by Vinit. V. Bidi and the team analyzed the potential of highway power generation using VAWT. The main purpose of the study was to fabricate the turbine at the lowest cost possible using the easily available material. The turbine was tested at the median of Highways accounting into power generation of 102.4 watts. The turbine rotated at 342rpm at a minimum speed of 12.77 (Vinit, et al., 2017).

In recent years, the affordable wind turbines-USA, Wind of Change-Germany, and Wind Side-Finland are some of the active organization manufacturing VAHWT. The first two have developed 3 range of VAHWT, 1 kW 3 bladed, 3kW 3 bladed, and 1 kW single-bladed turbines which are commercially available (Hockenos, 2019).

VAHWT though have been extensively used for small power production purpose, but it is still on research phase rather than commercial use due to its short fatigue life though it can withstand the wind of velocity 35m/s to 40 m/s and maximum up to 60 m/s. Under this thesis work, the rotor blade will be fabricated via RPM using the ABS plastic material because of complex blade geometry. The main purpose of the research work being analysis of the fabricated VAHWT, however further analysis will also make varying the aspect ratio of the rotor blade and maximum efficient design will be recommended. The rotor with maximum efficiency after assembling in the frame will be tested at the wind tunnel of Kathmandu University. The data obtained via experimental will be taken as reference for the data extraction via CFD and both data

are going to analyze and finally experimental verification will be performed. After that, the impact wind energy available at Sallaghari will be recorded and the performance of the proposed model on available impact wind energy will be carried out.

CHAPTER THREE: RESEARCH METHODOLOGY

The goal of this research work is to design, conduct numerical modeling and performance analysis of a highly efficient vertical axis helical wind turbine (VAHWT) suitable for highway application at Sallaghari that can generate power under the available impact wind energy at Sallaghari. Different steps that are involved in the design, simulation and performance analysis of VAHWT are listed as follows:
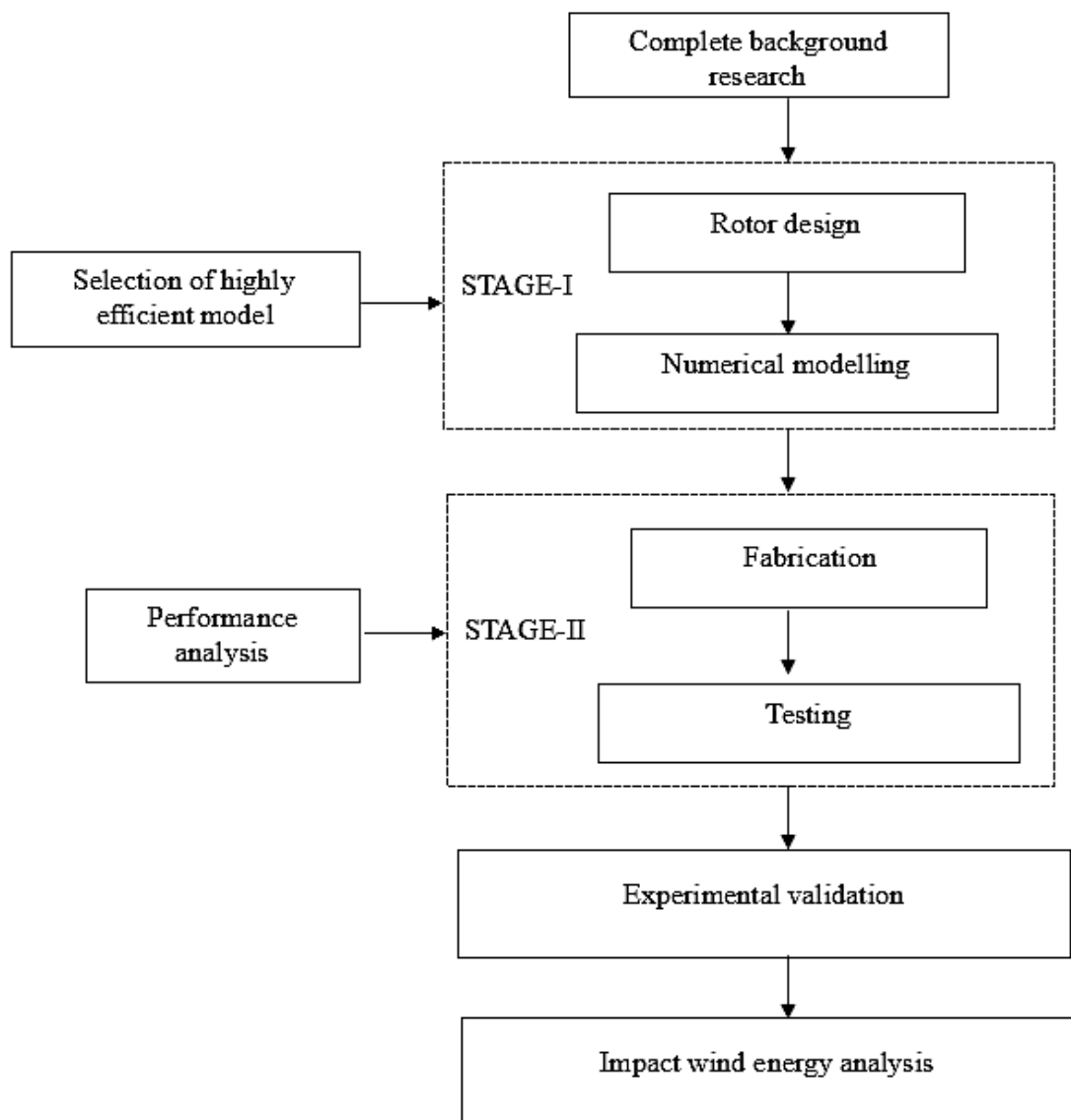
Figure 3.1: Different steps involved in design, fabrication and testing of VAHWT

The steps which are listed above are explained as follows.

3.1 Complete background research

Firstly, brainstorming was done about the possibility of the design and fabrication of VAHWT. After finding out its prospect and scope, it was finalized as the thesis work. For the same, Background research which includes reviewing a similar project done by different people in the past, research papers and different books related to helical wind turbines were studied thoroughly and the basis for the thesis work was built.

3.2 Design

After compiling background research, the information was analyzed. The design of the VAHWT rotor blade with all the necessary components of the turbine was designed based on a literature review on CATIA V5R20. There are several considerations and assumptions used under the design of the blade and shaft. These considerations are divided into two sections i.e. theoretical consideration and design considerations which are explained below.

3.2.1 Theoretical Considerations

Wind turbines extract energy from the wind stream by converting the kinetic energy of the wind to mechanical energy by the rotor and mechanical to electrical by the help of a generator. The following are the theoretical considerations used while doing calculations of power generation via theoretically and experimentally.

a) Power available in the wind

The theoretical power of impact wind energy available is given by,

$$\text{Kinetic Energy} = \frac{1}{2}mv^2 \qquad \text{...Eq. 3.1}$$

$$\text{Mass of Air transferring, } m = \rho Av \qquad \text{...............................Eq. 3.2}$$

Where,

m = mass of air transferring

Hence, the available power in the wind,

$$P_w = \frac{\rho A v^3}{2} \qquad \qquad \text{……………………….……..…….Eq. 3.3}$$

b) Power of the wind turbine

The power of the wind turbine can be calculated as follows:

$$P_t = \frac{1}{2}\rho A v^3 \times \eta_{wt} \qquad \qquad \text{………………………….………Eq. 3.4}$$

c) Rotor efficiency

The rotor efficiency of the turbine is expressed as follows.

$$\text{Efficiency, } \eta_{wt} = \frac{Pt}{Pw} \qquad \qquad \text{…………………………………….…Eq. 3.5}$$

d) Turbine Torque calculation

The torque is calculated as

$$T = \frac{60 \times Pt}{2\pi N} \qquad \qquad \text{………………………………………….Eq. 3.6}$$

Where,

ρ= Density of air, kg/m^3

A= Area of blade, m^2

V =Wind velocity, m/sec

T= Torque, Nm

N= Rotational speed, rpm

3.2.2 Design considerations

The design of VAHWT to be developed is partially based on WS-0, 15 developed by Windside. Wind Turbine Production Ltd Finland. The basic design considerations are:

A. Material choice: ABS Plastic

Aluminum is easily available, cheap material which can be fabricated easily but due to the complex geometry of the blade profile, the 3D-Printing machine is one of the ways to fabricate blade profile and locally available 3D-Printing machine normally use ABS Plastic material. Thus, ABS Plastic material is used to fabricate blade profile and cast

steel is used to build other components. The specifications of ABS Plastic are tabulated below.

Table 3.1: Specifications of ABS Plastic

Property	Value
Technical Name	Acrylonitrile butadiene styrene (ABS)
Chemical Formula	$(C_8H_8 \cdot C_4H_6 \cdot C_3H_3N)_n$
Tensile Strength	46 Mpa
Flexural Strength	74 Mpa
Specific Gravity	1.06

B. Blade dimension:

The tentative dimension of the helical rotor blade with varying aspect ratio is based on the following assumption. The wind tunnel available in Kathmandu University and Pulchowk campus is small in size i.e. Limited size.

Table 3.2: Design parameter of the helical blade

Property	Value
Coefficient of Performance	0.4
Angle of curvature	45^0
Expected power output	40W
Aspect ratio	Variable

C. Design of shaft

The diameter of the shaft couldn't be kept randomly as it has to bear the rotational torque. The design is based on the following assumptions which are tabulated below.

Table 3.3: Design parameter for shaft design

Property	Value
Max velocity	15 m/s
Factor of safety	5
Max revolution	1500 rpm

3.2.3 Rotor design

The helical rotor design and dimension was based on the speed of vehicles at Sallaghari highway. The basic schematic for the aerodynamic design of the vertical axis helical wind turbine is shown on the figure below.
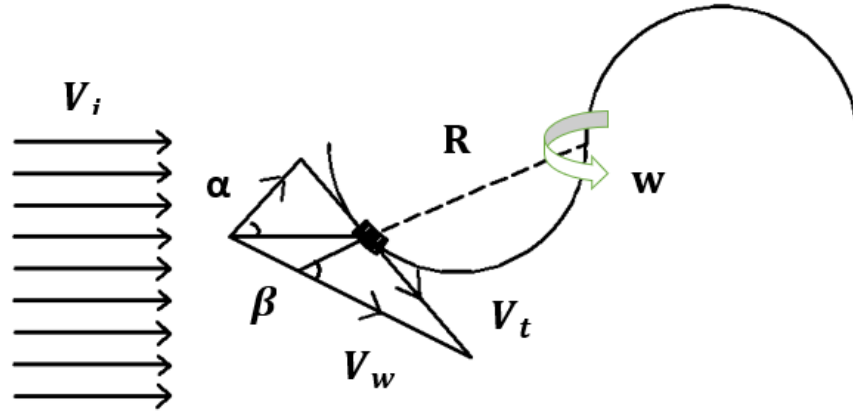
Figure 3.2: Velocities acting on the vertical axis helical wind turbine

The relative flow velocity and velocity in the tangential direction of the vertical axis helical wind turbine are defined in the below equations.

$$\vec{V_w} = \vec{V_i} \cos \alpha + \vec{V_t} \quad \text{..} \quad \text{Eq. 3.7}$$

$$V_t = \text{wr} \quad \text{...} \quad \text{Eq. 3.8}$$

$$A = \tan^{-1} \left(\frac{V_t}{V_i} \right) \text{...} \text{Eq. 3.9}$$

Where,

V_w = Relative flow velocity

V_i = Induced velocity

V_t = Velocity in the tangential direction

w = Rotor rotational speed

R = Helical rotor radius

The average speed of the vehicles is the prime factor to design the vertical axis helical wind turbine for highway applications. The questionnaire was done to determine the average vehicle speed at Sallaghari. It shows that the speed of the vehicles decreased from light to heavy vehicles or from two-wheeler to ten-wheeler vehicles. The average speed of the vehicles among all modes was 57 Km/hr.

27

Table 3.4: Speed of different vehicle modes at Sallaghari highway

S. N.	Vehicles speed at Sallaghari highway Km/hr			
	2-wheeler	4-wheeler	6-wheeler	10-wheeler
1	62	64	56	40
2	70	71	63	42
3	57	66	47	38
4	63	54	56	52
5	65	65	65	58
6	61	58	67	64
7	58	57	48	42
8	59	60	43	63
9	64	52	58	45
10	61	59	57	50
Maximum	70	71	67	64
Minimum	57	52	43	38
Average	62	60.6	56	49.4
Average speed among all vehicles type				**57**

The detailed blade design calculations are as follows:

From considerations,

Number of blade (N) = 2

Air density (ρ) = 1.225 kg/m^3

Coefficient of performance (C_p) = 0.4

Average velocity of vehicle on highways (V_o) = 57 km/hr

Angle of curvature = 45°

Expected power output (P_o) = 40w

Rotational speed of the designed turbine (w)= 104.719 rad/s

Using Eq. 3.7,3.8 and 3.9,

$A = \tan^{-1}(\frac{V_t}{V_i}) = \tan^{-1}(\frac{104.719 \times 188}{2000 \times 15.83})$ =31.874^o

$V_w = \sqrt{(V_i \cos\alpha)^2 + V_t^2}$

$$= \sqrt{(15.83\,Cos(31.874))^2 + (\frac{104.719 \times 188}{2000})^2}$$

$$= 16.667 \text{ m/s}$$

Now, Theoretical power $(P_w) = \dfrac{P_0}{C_p} = \dfrac{40}{0.4} = 100W$

For aspect ratio (AR) =1,

Swept area $(A_S) = H \times D = D^2$

Theoretical power $(P_w) = \dfrac{1}{2} \times \rho \times A_s \times V_w^3$

Or, $100 = \dfrac{1}{2} \times 1.225 \times D^2 \times 16.667^3$

Solving, we get

Diameter and height of rotor with aspect ratio 1 is given by,

D = 18.8 cm

H= 18.8 cm

Similarly, the detailed dimension of the blade with different aspect ratios is presented in the table below.

Table 3.5: Blades dimension

Aspect Ratio (AR)	Diameter (mm)	Height (mm)
0.8	209.8	168
0.9	197.8	178.1
1	188	188
1.1	179	197
1.2	171	205
1.3	165	215
1.4	159	223
1.5	153	230

The detailed design of the rotor blade and assembly has been completed in CATIA V5R20 based on the above design parameters and specifications. The detailed design

process is presented in the methodology section where the final assembly was saved in "*.igs" format for further simulation in the ANSYS workbench.
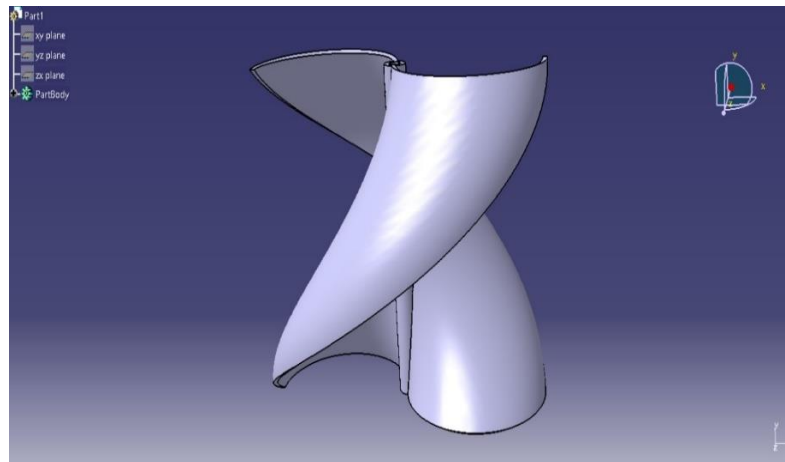
Figure 3.3: Design of VAHWT in CATIA V5R20

3.2.3 Design of Shaft

The diameter of the shaft couldn't be kept randomly as it had to bear the rotational torque. The design is based on the following considerations and calculations.

Some assumptions made before the design is:

Max velocity = 15m/s

The factor of safety = 5

Max revolution = 1500 rpm

Now, based on the above assumptions, calculating the power and tensile strength as:

$$\text{Power (P)} = \frac{1}{2} \times \rho \times A \times V^3$$

$$= 100 \text{ W}$$

As Ultimate tensile strength of ABS Plastic material used in the turbine is 46 mpa

$$\text{So,} \qquad P = \frac{2\pi nt}{60}$$

$$\Rightarrow \quad T = 0.63694 \text{ Nm}$$

As we know,

$$T \times FOS = \frac{\pi}{16} \times d^3 \times \tau$$

$$\therefore \quad d = 7.0659 \text{ mm} \approx 7.1 \text{ mm}$$

Hence, from the above calculation, the approximate diameter of the shaft is found to be 7.1mm. During the fabrication, the shaft of 7.1mm dia. Is found to be infeasible due to lack of availability of material and machining difficulties. Thus, for convenience, the diameter of 8 mm has been used for the final model fabricated.

3.3 Numerical Modelling

Simulation of the VAHWT designed on CATIA V5R20 was performed on ANSYS Workbench 18.1. The Simulation of VAHWT to be developed is based on the following considerations:

- **Software available**: Abacus, Psunami, openfoam, Autodesk CFD, simscale CFD, ANSYS Fluid-Flow (Fluent) etc.

- **Software chosen**: ANSYS Fluid (Fluent) V18.1

- **Turbulence Model**: SST model

- **Operations performed**: Wind flow analysis, Speed-Torque variation

The experimental data were taken as a reference parameter for the numerical modeling on ANSYS Workbench 18.1. The inlet velocity and reference rotational speed were taken at the initial phase. The pressure output was taken atmospheric pressure and the wall was taken as no-slip conditions. The boundary conditions are tabulated below.

Boundary Condition:

Analysis type	:	Transient Analysis
Domain		
Fluid	:	Air
Reference Pressure	:	1 atm
Blade Material	:	Acrylonitrile Butadiene Styrene Plastic $(C_8H_8 \cdot C_4H_6 \cdot C_3H_3N)_n$
Turbulence Model	:	SST model
Inlet Condition		
Air velocity	:	5m/s for comparing between different models and 4.4 to 11 m/s velocities for experimental model
Inlet condition	:	Velocity inlet

| Outlet Condition | : | Pressure outlet |
| Wall condition | : | Stationary wall |

For the numerical analysis of the proposed model rotor, the CATIA file was imported in ANSYS design modeler for geometrical setup and other preprocessing and processing works are explained below.

a) Numerical modeling setup

The proposed model rotor was simulated by using several design considerations. Some parameters which were considered under the numerical modeling section are explained below:

- **Geometry**

The numerical modeling was performed by using ANSYS Workbench 18.1 to understand the pressure distribution and torque generated by the various helical blades. The 3D proposed model was created in CATIA V5R20 and it was imported in ANSYS Design modeler. To create the fluid region, enclosure and Boolean features were used. For transient three-dimensional analysis of VAHWT, two separate fluid domains are needed for simulation. For this analysis, two enclosure of box and cylindrical type were used in which box type shows the wind tunnel stationary domain and the cylindrical type shows the rotating domain. To create the fluid domain, subtract type Boolean was used.
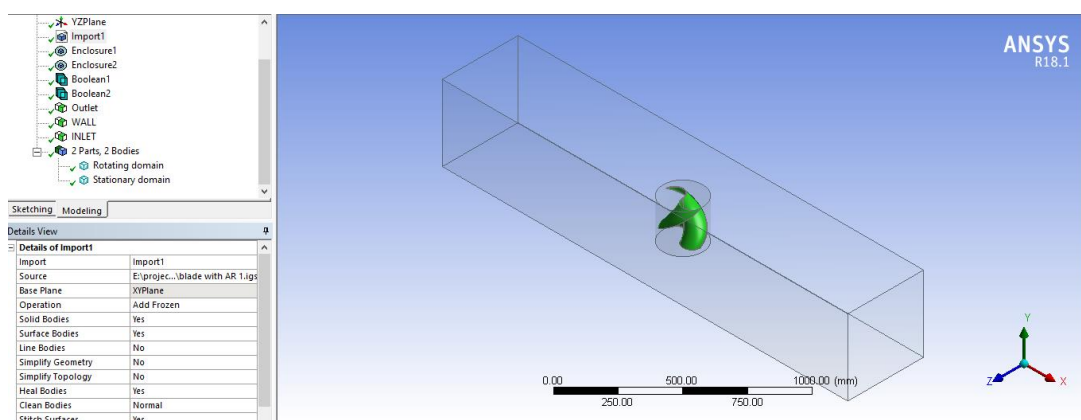
Figure 3.4: Geometry setup of the proposed model on ANSYS Workbench 18.1

32

- **Mesh**

As the geometry of VAHWT is complicated automatic meshing in ANSYS workbench was used resulting in the formation of tetrahedral elements. The meshing process involved the use of both global meshing controls as well as local meshing controls. The local controls used for developing the mesh were faced sizing and body sizing.
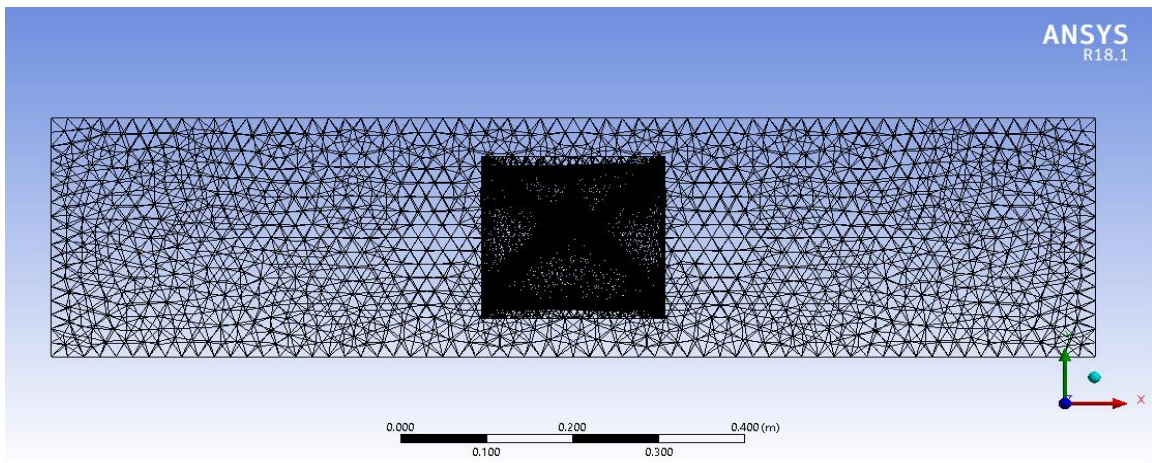
Figure 3.5: Wind tunnel with meshing
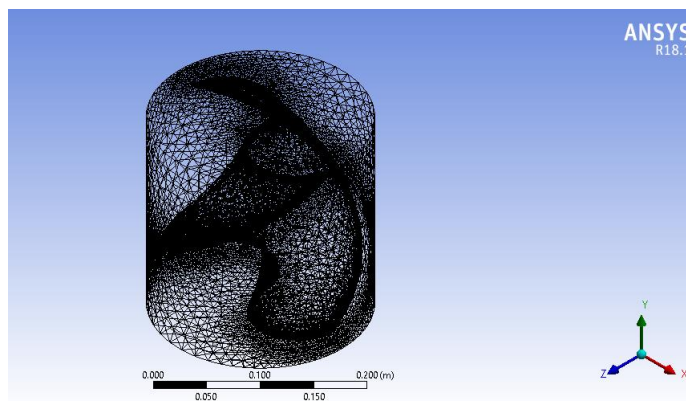
Figure 3.6: Cylindrical enclosure and rotor with meshing

- **Model Setup**

The next step after creating the appropriate and suitable meshes is specifying the stationary and rotating domain, boundary conditions such as inlet velocity and reference rotational speed, analysis type etc. To solve the problem, it is necessary to create at least

two types of domains that are stationary and rotating. The box-type enclosure i.e. Wind tunnel is considered as a stationary domain whereas the rotor is inserted in the rotating domain.

Figure 3.7: Domains in ANSYS Workbench 18.1

➢ The turbulence model for both stationary and rotating domain has been chosen shear stress transport (SST) model. Second-order upwind based discretization and the double-precision option were used for mean flow, turbulence, and transition equations for better, stable and highly accurate results.

➢ Boundary conditions for the simulations such as inlet velocity and reference rotational speed were taken from experiments on wind tunnel testing. The blade walls were given a no-slip condition and zero rotational velocity relative to the sliding mesh zone.

➢ The reference rotational speed was chosen from the experimental method i.e. Wind tunnel testing method. Convergence criteria are kept consistent throughout the study requiring all 5 residuals to decrease to a value of 1e-04.

- **Time step size calculation**

Smaller the time step size may increase the accuracy but computational time also increases. The following steps help to know the time step size calculation for the numerical analysis of the proposed model.

The reference rotational speed = 300 rpm

(300 rotations / min) × (1 min / 60 sec) = 5 rotations / sec

(5 rotations / sec)$^{-1}$ = 0.2 seconds / rotation

Now, Time required for every 10^0 of rotation = $\frac{0.2}{36}$ = 0.005556 sec

Therefore, 0.005556 sec gives 1-time step for every 10 degrees of rotation and 72-time steps gives 2 full rotations.

b) Mesh independence Test

The Mesh independence test is one of the tests that allow reducing the mesh size and computational time without losing accuracy. For the mesh independence test, the different meshing elements was varying from coarse mesh to fine mesh to get the better result. The table below gives information about different torque available with respect to different meshing elements.

Table 3.6: Number of element vs torque for mesh independence test

No. Of elements	Torque (Nm)	Convergence Iteration
43219	0.0157	1910
52847	0.0245	1952
90909	0.0245	1972
146002	0.0250	1988
350418	0.0257	1991
572230	0.0257	1995
810548	0.0259	1997
956943	0.0259	2016
1120934	0.0259	2019

The above table shows that the finer the mesh, the higher the convergence iteration i.e. More time required to get the solution. By using several simulation considerations, the numerical modeling of the proposed model rotor was done in ANSYS Workbench 18.1. The detailed rotor simulation considerations and calculations are as follows:

Reference rotational speed (N) = 300 rpm

Wind tunnel inlet velocity (V_i) = 5 m/s

For rotor with aspect ratio 1,

Diameter = 18.8 cm

Height = 18.8 cm

Swept area $(A_s) = D \times H = 18.8 \times 18.8$

$$= 0.035344 \text{ m}^2$$

Torque calculated via simulation (T) = 0.033849687 Nm

From Eq. 3.4, Theoretical Power $(P_w) = \frac{1}{2} \times \rho \times A_s \times V_i^3$

$$= \frac{1}{2} \times 1.225 \times 0.035344 \times 5^3$$

$$= 2.706025 \text{ W}$$

Actual Power $(P) = \frac{2\pi nt}{60}$

$$= \frac{2\pi \times 300 \times 0.033849687}{60}$$

$$= 1.06341928$$

From Eq. 3.6, Coefficient of performance $(C_p) = \frac{P}{P_w}$

$$= \frac{1.06341928}{2.706025}$$

$$= 0.3927$$

After the complete simulation, the torque developed by the turbine rotor was calculated which is used to generate the performance coefficient of the rotor. It was found that the rotor with aspect ratio 1 had a maximum performance coefficient i.e. Efficiency with 39.27%. Similarly, the coefficient of performance calculation with different aspect ratios is presented in the table below.

Table 3.7: Simulation calculations of different blades at 5 m/s

AR	D (mm)	H (mm)	V_i (m/s)	Moment (Nm)	Moment coefficient (C_m)	Power output (P_{CFD})	Theoretical power (P_{th})	Performance coefficient (C_p)
0.8	209.8	168	5	0.02544	0.001661	0.7988	2.6985	0.2960
0.9	197.8	178.1	5	0.02378	0.001553	0.7470	2.6971	0.2769
1	188	188	5	0.03384	0.002210	1.0628	2.7060	0.3927
1.1	179	197	5	0.02539	0.001924	0.7973	2.6998	0.2953
1.2	171	205	5	0.02430	0.001587	0.7631	2.6838	0.2843
1.3	165	215	5	0.02371	0.001548	0.7446	2.7160	0.2741
1.4	159	223	5	0.01907	0.001429	0.5991	2.7146	0.2206
1.5	153	230	5	0.02206	0.001646	0.6927	2.6942	0.2571

After calculating the performance coefficient of all the rotors with varying aspect ratios, the highly efficient model was simulating on varying inlet velocity and rotational speed. The below table 3.8 gives information about generated torque at different inlet velocity via numerical modeling of the rotor of aspect ratio 1 at 300 rpm. It shows that the inlet velocity of the tunnel is directly proportional to the torque generated by the rotor blade i.e. The torque generated by the rotor increases sharply with respect to increase in inlet velocity.

Table 3.8: Torque generated with respect to inlet velocity of the blade at 300 rpm

Velocity(m/s)	Generated Torque (Nm)
5	0.03384
6	0.03725
7	0.05475
8	0.07389
9	0.09050
10	0.10843

The below table 3.9 illustrates about generated torque at different rotational speed of rotor via numerical modeling of the rotor of aspect ratio 1 at 5.8346 m/s i.e. Average speed of impact wind energy at Sallaghari.

Table 3.9: Torque generated with respect to RPM of the rotor at 5.8346 m/s

Rotational speed (rpm)	Torque generated (Nm)
300	0.03433
350	0.04273
400	0.04814
450	0.04966
500	0.04491
550	0.04670
600	0.04312

3.4 Fabrication

The fabrication of the rotor blade was performed in the Rapid Prototyping Machine (RPM) situated at Zener Technologies, Kupondole. The design made in CATIA was used as a reference to fabricate the rotor through a rapid prototyping machine. The process of printing took almost 17 hours to completely fabricated because of the complexity in the geometry of the blade. The material available there was ABS plastic; using which the fabrication was completed. The various factors such as the complex geometry of the rotor blade, lack of machines to fabricate the rotor blade in the near vicinity, lack of availability of proper material etc. Were prime reasons to choose this method of fabrication.
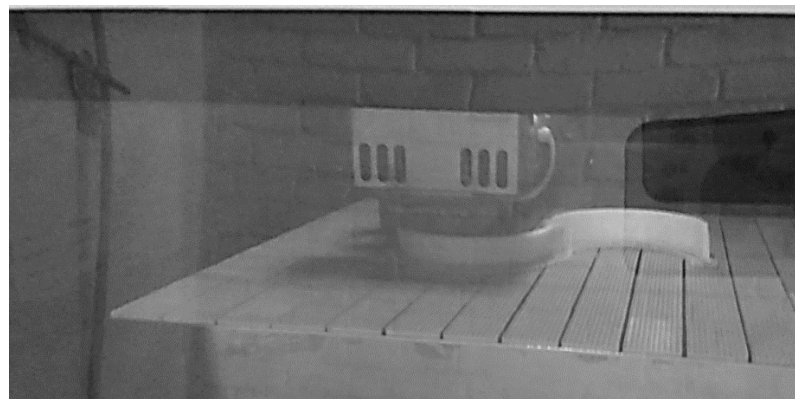
Figure 3.8: Printing of rotor blade of VAHWT using RPM at Zener Tech, Kupandol

The frame to stand the rotor blade was fabricated using cast iron. The black sheet made of cast iron was used for base known as Bed. Two cast iron threaded bolt were used to make the column and they were welded to make the frame stable. The main shaft of the rotor blade was supported by the two bearings of bearing rating 608ZS. Two equal sizes of plastic gear were used for coupling between the rotor shaft and the generator shaft. The detailed summary of the material along with dimension that was used are tabulated below.

Table 3.10: Different parts with their material type and dimension

S. N.	Part Name	Material	Dimension
1	Bed	Cast Iron	300 mm x100 mm x10 mm
3	Column	Mild Steel	D14 x 350 mm
4	Generator	Mild Steel	DC Motor
5	Shaft	Mild Steel	Height=250mm, Dia.=8 mm
6	Rotor	ABS	188mmx188mm
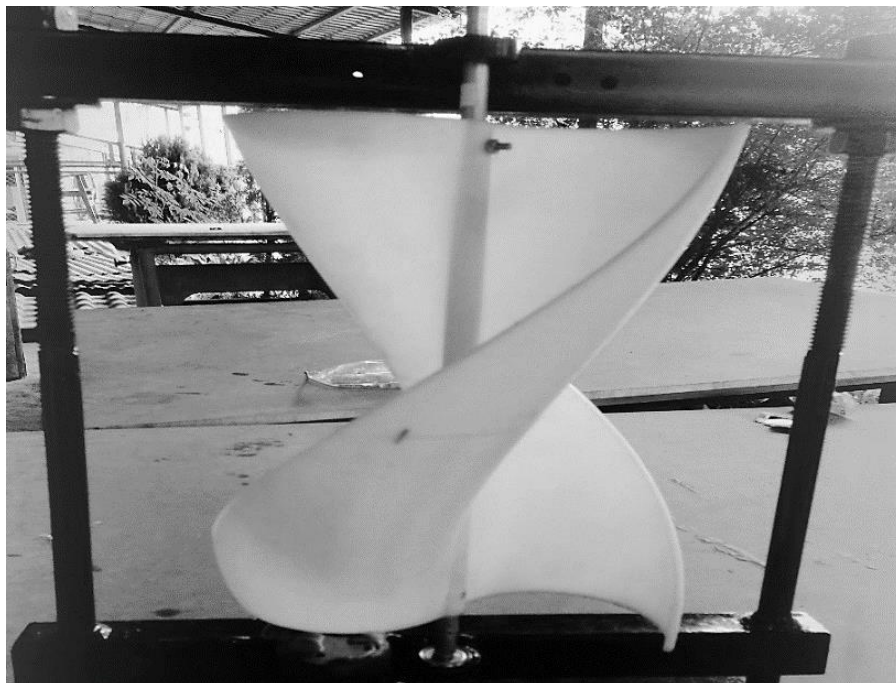
Figure 3.9: Fabricated vertical axis helical wind turbine with a frame

3.5 Wind tunnel testing

The testing of the fabricated model of VAHWT was tested at KU. The various setups were made for better results via testing which is included in this chapter. This chapter deals with the machinery tools, instruments, and setups that were required and prepared for the testing. They are as follows:

    A. Measuring instruments
    B. Wind tunnel test rig
    C. Experimental process

All the machinery tools, instruments and setups that were required and prepared for the testing are explained below.

3.5.1 Measuring Instruments

Various instruments used to measure the parameters like rpm, wind speed, current and voltage are as follows:

    a. Digital tachometer
    b. Digital anemometer
    c. Digital multimeter

These instruments are explained below:

A. Digital tachometer

A tachometer is an instrument measuring the rotation speed of a shaft. The device usually displays the revolutions per minute (RPM) on a calibrated display screen. The tachometer counts the no of times light reflected from the sticker attached to the shaft and displays the result. The tachometer used for this experimental setup was the DT2234B model.

Figure 3.10: Digital tachometer

B. Digital anemometer

An anemometer is a device used for measuring wind speed. A digital type anemometer was used to measure the wind speed inside the tunnel. The anemometer used was a handheld digital anemometer, which consists of a small fan that rotates in the wind and displays the result in the digital screen. The anemometer used for this experimental measurement was AM-4201 model.

Figure 3.11: Digital anemometer

C. Digital multimeter

A Multimeter is an electronic measuring instrument. A digital multimeter can measure voltage, current, resistance and continuity. The digital type Multimeter was used for the measurement of voltage and current generated by the DC generator.
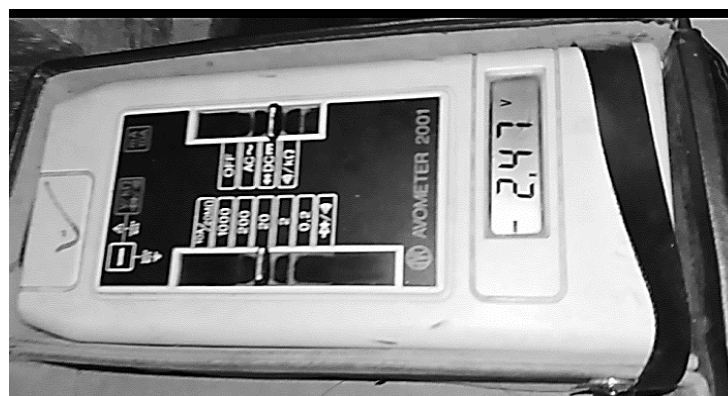
Figure 3.12: Digital multimeter

3.5.2 Wind Tunnel Test Rig

A wind tunnel consists of a rectangular passage with the object under test mounted in the test rig section. Air is made to move past the object by a powerful fan system or other means. The wind tunnel used for testing was a student project of Kathmandu University, which was made up of wood and tin sheet. A powerful axial fan is attached to one end. The total length of the wind tunnel is 209 cm. The tubular passage is 40*40 cm^2 and the opening ends (nozzle and diffuser section) on both sides are 70*70 cm^2. The honeycomb is attached in the tubular passage to make the flow of air in a streamline and convert the disturbed flow to laminar flow. Towards the end of the tubular passage, there is a test stand section surrounded all the sides by glass frames to make it visible during the test.

Figure 3.13: Image of Wind tunnel of Kathmandu University

3.5.3 Experiment Setup

The testing of the fabricated model was done at Kathmandu University. The existing wind tunnel test rig was used for the testing of the model. The speed of the wind was varied from 3m/s to 11m/s.

Figure 3.14: Schematic diagram of the wind tunnel of KU with labeling

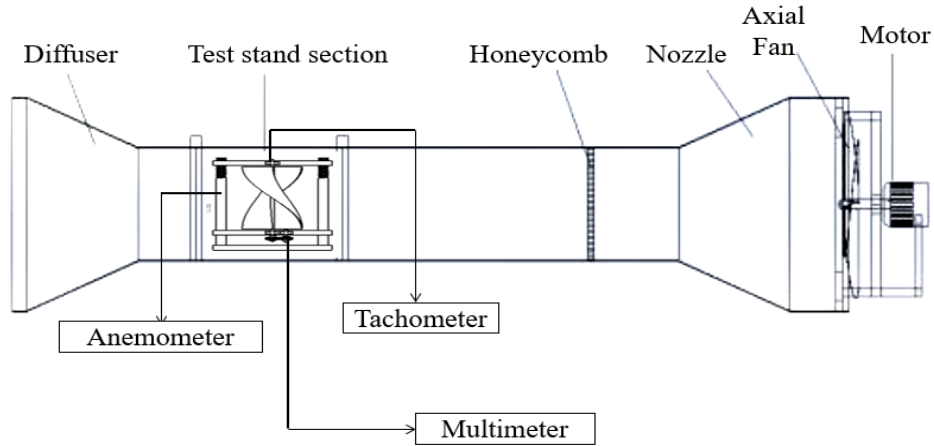The rpm of the rotor was measured along with the wind velocity at the corresponding time by using a digital tachometer. The poor knob adjustment to control the speed of the axial fan in the wind tunnel caused the variation in the wind velocity at the same knob adjustment. The velocity measured via anemometer seemed fluctuating despite adjusting the knob at one point. Thus 9 experiments with 20 sample readings were taken and average data was considered. The detailed tabulated values of wind speed measured by Anemometer and RPM of the rotor measured by the Tachometer is shown in table 1 of Annex A. These data were recorded at the first stage of testing.

Table 3.11: Summary table of recorded wind velocity and rotational speed

S. N.	Average Velocity	Average rpm	Tip speed ratio	Max Velocity	Max rpm	Min Velocity	Min rpm
1.	3.89	180.95	0.457895	4.263	200.2	3.59	156
2.	4.74	221.43	0.459848	4.93	241	4.3	206.2
3.	5.36	278.9	0.512201	5.8	317	4.91	251
4.	6.28	337.13	0.528438	6.75	359.6	5.91	315.6
5.	7.3	381.38	0.51427	7.62	410.6	6.82	358.4
6.	8	462.34	0.56889	8.49	489.9	4.45	417.3
7.	9.44	555.55	0.579305	9.8	596.4	8.9	504
8.	10	647.25	0.637131	10.45	688	9.5	598.6
9.	11.2	690	0.60644	11.51	708.2	11.1	675.8

From the above table, it can be found that the rpm of the rotor has been increased while increasing the inlet velocity of the wind tunnel. The poor knob adjustment potentiometer to control the speed of the axial fan in the wind tunnel caused the variation in the wind tunnel inlet velocity at the same knob adjustment. The inlet velocity of the wind tunnel measured by using an anemometer seemed fluctuating despite adjusting the knob at one point. Thus 9 experiments with 20 sample readings were taken and average data was considered. The maximum velocity recorded was 11.51 m/s and the corresponding rpm of the rotor was recorded to be 708.2 rpm as measured by the tachometer.

Figure 3.15: Experiment measurement of inlet velocity and rotational speed

The experiment was carried out in the Kathmandu University wind tunnel and the details procedure of experimental section for power measurement was listed below.

- Firstly, the fabricated proposed model rotor was placed at the test rig section of the wind tunnel which have a rectangular passage of 40*40 cm^2.
- Usually, the generated torque of the rotor was measured by torque sensor. But due to unavailability of torque sensor, multimeter was used for power measurement.
- The air with different varying inlet velocity was passed by using axial fan and potentiometer. The inlet velocity was measured by using anemometer.
- The honeycomb is attached in the tubular passage to make the flow of air in a streamline and convert the disturbed flow to laminar flow.
- The poor knob adjustment potentiometer to control the speed of the axial fan in the wind tunnel caused the variation in the wind tunnel inlet velocity at the same knob

adjustment. Thus 9 experiments with 20 sample readings were taken and average data was considered.

- The dc motor was used as a generator and generated power and rotational speed was measured by using digital multimeter and tachometer.

- The locally available dc generator was used for power generation. Therefore, the generated torque is the combined torque of rotor and generator. For rotor torque calculation, generated torque was considered as the rotor torque due to torque measurement instrument unavailability i.e. the losses on the generator was neglected.

- Multimeter was used to calculate the current and voltage produced by the fabricated model and the power generated was calculated by multiplying both voltage and current.

- The torque generated is a function of output power and rotational torque which is shown in Eq. 3.6 in theoretical consideration section.

- The torque generated by the rotor was calculated by using Eq. 3.6 by using both power output and rotational speed recorded and theoretical power was calculated by using recorded inlet velocity of the air.

The current and voltage generated by the rotor at various wind velocity was recorded as shown in the table below. The power generated was calculated by multiplying both voltage and current. The torque generated by the proposed model turbine by the experimental method was calculated by using Eq. 3.6 in the theoretical considerations section. This table shows the power produced by the fabricated model in wind tunnel and power produced by the same model theoretically. The theoretical power should always be higher than the actual power and a similar condition can be observed in the below table too. The performance coefficient via the experiment was calculated by using Eq. 3.5. The experimental performance coefficient was varied from 0.15 to 0.27 which seems almost relevant in terms of fluctuation.

Table 3.12: Performance Coefficient of the fabricated model via testing

Exp.	Velocity (m/s)	rpm	Voltage (V)	Current (A)	P_{Exp} (W)	P_{Th} (W)	Exp. Torque (Nm)	C_p (Exp.)
1	4.41	190.3	1.22	0.24	0.2928	1.85668	0.01470	0.15770
2	5.13	250.9	1.48	0.31	0.4588	2.92263	0.01747	0.15698
3	6.05	310.4	2.03	0.41	0.8323	4.79389	0.02562	0.17362
4	6.81	355	2.54	0.51	1.2954	6.83696	0.03486	0.18947
5	7.54	402.5	3.13	0.65	2.0345	9.27974	0.04829	0.21924
6	8	455	3.44	0.77	2.6488	11.08388	0.05562	0.23898
7	9.26	519	4.14	1.05	4.347	17.18916	0.08002	0.25289
8	10.1	569	4.72	1.23	5.8056	22.30416	0.09748	0.26029
9	11	640	5.28	1.47	7.7616	28.81375	0.11587	0.26937

At the same wind velocity as the wind tunnel, the fabricated model was simulated on ANSYS Workbench 18.1 and the same velocity and rotational speed from the experiment were taken as an input parameter for the numerical modeling of the proposed model.

Table 3.13: Performance Coefficient of the fabricated model via numerical modeling

Exp.	Velocity (m/s)	rpm	P_{Th} (W)	CFD Torque (Nm)	P_{CFD} (W)	C_p (CFD)
1	4.41	190.3	0.29402	0.01557	0.31022	0.16708
2	5.13	250.9	0.46324	0.02687	0.70561	0.24143
3	6.05	310.4	0.84448	0.04384	1.42441	0.29713
4	6.81	355	1.30048	0.05847	2.17246	0.31775
5	7.54	402.5	2.03763	0.07341	3.09264	0.33327
6	8	455	2.65568	0.08140	3.87663	0.34975
7	9.26	519	4.3677	0.11391	6.18778	0.35998
8	10.1	569	5.82448	0.13485	8.03106	0.36007
9	11	640	7.788	0.15203	10.18390	0.35344

This above table 3.13 shows the power produced by the fabricated model via numerical modeling on ANSYS Workbench 18.1 and power produced by the same model theoretically. The theoretical power should always be higher than the numerical modeling power and a similar condition can be observed in the above table too. The performance coefficient via simulation was calculated. The simulation performance coefficient was varied from 0.16 to 0.36 which seems almost relevant in terms of fluctuation.

3.5.4 Uncertainty analysis

Uncertainty analysis is one of the mathematical models for error analysis under the experimental section. Under the wind tunnel testing method, the multimeter was used for power measurement in terms of voltage and current. Therefore, the power measurement is the function of voltage and current. And the least count of multimeter while measuring the voltage and current is 0.01. The details calculation part of the error analysis is explained below.

$P = f(V, I)$

$$\sigma_p = \pm \sqrt{\left(\frac{\partial p}{\partial V} \sigma_V\right)^2 + \left(\frac{\partial p}{\partial I} \sigma_I\right)^2}$$

where,

σ_p = Standard deviation of power measurement

σ_V = Least count of multimeter while measuring the voltage

σ_I = Least count of multimeter while measuring the current

As we know,

$$\frac{\partial p}{\partial V} = \text{I}$$

$$\frac{\partial p}{\partial I} = \text{V}$$

$$\sigma_p = \pm \sqrt{(I \times \sigma_V)^2 + (V \times \sigma_I)^2}$$

$$= \pm \sqrt{(0.241 \times 0.01)^2 + (1.22 \times 0.01)^2} = \pm 0.0124$$

Similarly, the error percentage was calculated at different power measurement were tabulated below.

Table 3.14: Error percentage calculation at different power measurement

Voltage (V)	Current (A)	Power (W)	σ_p	% error
1.22	0.24	0.2928	0.0124	4.25
1.48	0.31	0.4588	0.0151	3.30
2.03	0.41	0.8323	0.0207	2.49
2.54	0.51	1.2954	0.0259	2.00
3.13	0.65	2.0345	0.0320	1.57
3.44	0.77	2.6488	0.0353	1.33
4.14	1.05	4.347	0.0427	0.98
4.72	1.23	5.8056	0.0488	0.84
5.28	1.47	7.7616	0.0548	0.71

3.6 Performance Analysis

The performance analysis of vertical axis helical wind turbine was carried out by making different curve. These curves are between

- Wind speed and revolution
- Wind speed and power output
- Theoretical power and actual power at different wind speed
- Aspect ratio and power coefficient

The data obtained from the testing and ANSYS workbench were used to generate the various charts and graphs to derive the final conclusion. The entire performance analysis was entirely based only on the data generated through testing and fabrication.

3.7 Impact wind energy measurement at Sallaghari

The Highway potential analysis of vertical axis helical wind turbines was carried out at Sallaghari, Bhaktapur because very much less work has been done in the impact energy sector. As the automobiles move on different highways, there is a creation of front and back pressure columns on both sides of the roads. Due to this pressure column, the creation of pressure thrust and flow of impact wind energy occurred. This Impact wind energy mainly depends on the following factors:

a) The intensity of the vehicles traffic
b) Size and shape of the vehicles
c) Speed of the vehicles
d) Distance between rotor and vehicles
e) Impact angle
f) Natural wind speed

Figure 3.16: The location of the impact wind energy measurement at Sallaghari by using google earth

The pressure thrust created by the pressure column on both sides of the road can be converted into mechanical energy by the help of the proposed rotor and this mechanical

energy can be converted into electrical energy by the help of a generator placed at the divider of the highways. The impact wind energy available at Sallaghari was investigated to understand the pattern of impact wind energy available on highways.

Figure 3.17: Impact wind energy measurement at Sallaghari

The impact wind energy at Sallaghari highway was recorded to predict impact wind energy available at 1.5m height from the road level. The detail table B.1 is at appendix B which contains the different impact wind speed recorded throughout the day for different ten days while the summarized data of velocity of impact wind energy available at Sallaghari highway are tabulated in the following table.

Table 3.15: Velocity of impact wind energy at Sallaghari highway

S.N.	1.5m height of anemometer from road level		
	Time	Velocity of impact wind energy (m/s)	Average Velocity
1	7:00 AM	4.5	5.8346
2	8:00 AM	7.61	
3	9:00 AM	6.73	
4	10:00 AM	7.31	
5	11:00 AM	5.84	
6	12:00 PM	5.1	
7	1:00 PM	5.2	
8	2:00 PM	3.95	
9	3:00 PM	5.4	
10	4:00 PM	7.86	
11	5:00 PM	6.91	
12	6:00 PM	4.42	
13	7:00 PM	5.02	

Measurements of impact wind energy potential usually done by using an anemometer and the reference rotational speed of the rotor were calculated by the help of a mathematical interpolation function. The curve between wind speed and rotational speed is a nearly straight line. Therefore, a two-point interpolation function was used for calculation of the respective rotational speed of the turbine with respect to the impact wind energy available at Sallaghari which is shown in figure C.1 in Appendix C section. Then, these data can be used as a reference signal for numerical analysis of the proposed model in ANSYS Workbench 18.1. The table below gives information about the available impact wind energy at Sallaghari with respect to different impact wind speed.

Table 3.16: Power generated by the turbine with respect to impact wind speed available at Sallaghari using ANSYS Workbench 18.1

S.N.	Time	Velocity of impact wind energy m/s	Rotational Speed Rpm	CFD Moment Nm	Power generated W	Average Power W
1	7:00 AM	4.5	210	0.0226621	0.4983	
2	8:00 AM	7.61	417.23	0.0700463	3.0604	
3	9:00 AM	6.73	356.65	0.0581739	2.1726	
4	10:00 AM	7.31	382.53	0.0682792	2.7351	
5	11:00 AM	5.84	309.28	0.0454043	1.4705	
6	12:00 PM	5.1	254.8	0.0285332	0.7613	
7	1:00 PM	5.2	264.06	0.0327664	0.9060	1.5312
8	2:00 PM	3.95	183.8	0.0122404	0.2355	
9	3:00 PM	5.4	282.6	0.0365640	1.0820	
10	4:00 PM	7.86	446.14	0.0741420	3.4638	
11	5:00 PM	6.91	364.46	0.0629082	2.4009	
12	6:00 PM	4.42	206.2	0.0200399	0.4327	
13	7:00 PM	5.02	247.38	0.0265020	0.6865	

CHAPTER FOUR: RESULT AND DISCUSSION

4.1 Result via CFD Analysis

The data obtained from the ANSYS Workbench 18.1 are listed as follows:

a) Mesh Independence Test

b) Effect in performance coefficient of VAHWT with varying aspect ratio(D/H)

c) Effect in torque generated of the helical rotor with varying inlet velocity and rotational speed on ANSYS Workbench 18.1

d) Static pressure and velocity distribution on rotor blade with aspect ratio 1

Above listed data obtained via ANSYS Workbench 18.1 are explained as follows:

a) Mesh independence Test

The Mesh independence test is one of the tests that allow to reduce the mesh size and computational time without losing accuracy. For the mesh independence test, the different meshing elements was varying from coarse mesh to fine mesh to get the better result.
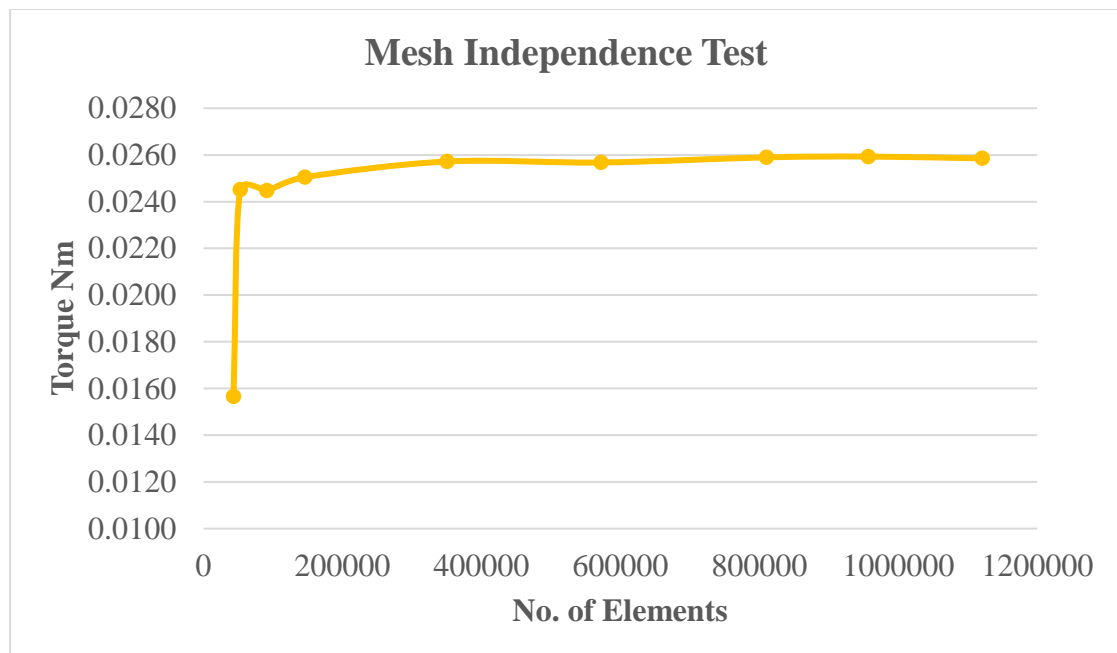
Figure 4.1: Torque vs number of elements for mesh independence test

When the mesh size is course enough, there are differences in results. Finer the mesh size, there exists a limit beyond which there are no changes in the results even though the mesh size will be very much fine. The above figure illustrates that when the mesh size is course i.e. 43219 number of elements which gave very low torque of 0.0157 Nm. After making finer mesh, the generated torque increased. Beyond the 810548 number of elements, there are no changes in the results i.e. Torque with 0.0259 Nm. Therefore, the mesh with 810548 elements is enough to get accurate results.

The detailed simulation of the rotor was conducted on ANSYS Workbench 18.1 based on the above simulation consideration. The number of nodes and elements of the rotor with different aspect ratio was calculated and tabulated below:

Table 4.1: Calculations of different mesh density

AR	D (mm)	H (mm)	Mesh		Skewness	Orthogonal Quality
			Nodes	Elements		
0.8	209.8	168	200196	1096098	0.84748	0.99531
0.9	197.8	178.1	203354	1114239	0.84311	0.99824
1	188	188	204394	1121005	0.84778	0.99757
1.1	179	197	206476	1132915	0.84948	0.99595
1.2	171	205	209111	1148055	0.84731	0.99764
1.3	165	215	210019	1152976	0.84606	0.99736
1.4	159	223	210972	1158474	0.84908	0.99595
1.5	153	230	211085	1159006	0.84984	0.99459

b) **Effect in performance coefficient of VAHWT with varying aspect ratio(H/D)**

The figure below shows the variation of performance coefficient of vertical axis helical wind turbine with respect to their aspect ratio.
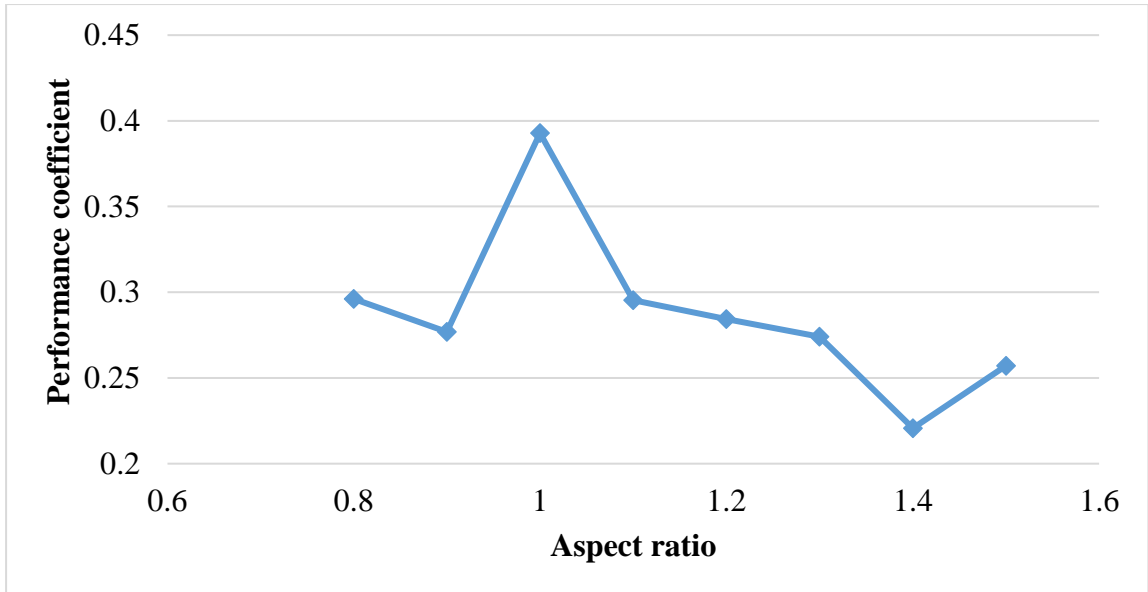
Figure 4.2: Aspect ratio vs performance coefficient in different models

The simulation was done on ANSYS Workbench 18.1 for all the rotors with varying aspect ratios. The above figure shows that the performance coefficient was not followed any trend because there is a variation on both the diameter and height of all the rotors. Due to variation on both diameter and height, there was a fluctuation in the performance coefficient. The data generated from CFD; it can be noticed that the aspect ratio of 1 has a maximum performance coefficient of 0.3927. Thus, the rotor with aspect ratio 1 could be the most economical wind turbine in terms of their power generation and efficiency of the turbine.

c) **Effect in torque generated of helical rotor with varying inlet velocity and rotational speed on ANSYS Workbench 18.1**

The figure gives information about the torque generated by the blade with aspect ratio 1 with respect to different wind speed at 300 rpm. It shows that the torque generated by the rotor blade is directly proportional to the impact velocity of the wind. Firstly, the torque generated is slightly increased from 5 to 6 m/s due to the rpm of the blade is near to 300 rpm. After that, the torque generated increased sharply due to a large variation of the rotational speed of the blade rather than 300rpm.
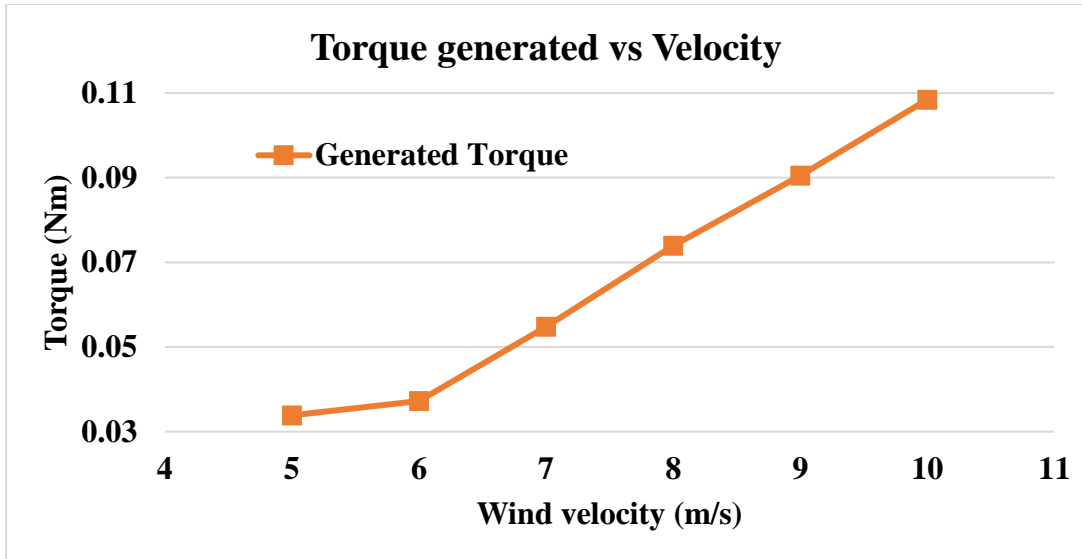
Figure 4.3: Torque vs inlet velocity of blade with aspect ratio 1 at 300 rpm

The below figure illustrates about generated torque at a different rotational speed of rotor via numerical modeling of the rotor of aspect ratio 1 at 5.8346 m/s i.e. Average speed of impact wind energy at Sallaghari. It shows that the torque generated started sharply increased with respect to rotational speed, reaching a peak of 0.049661001 Nm at 450 rpm. It then decreased because the rotational speed of the rotor varies from 450 to 600 at the velocity of 5.83 m/s which was higher rotational speed than the maximum possible experimental rotational speed. Therefore, while increasing the rotational speed of the blade, there was a decreasing trend of the torque occurred.
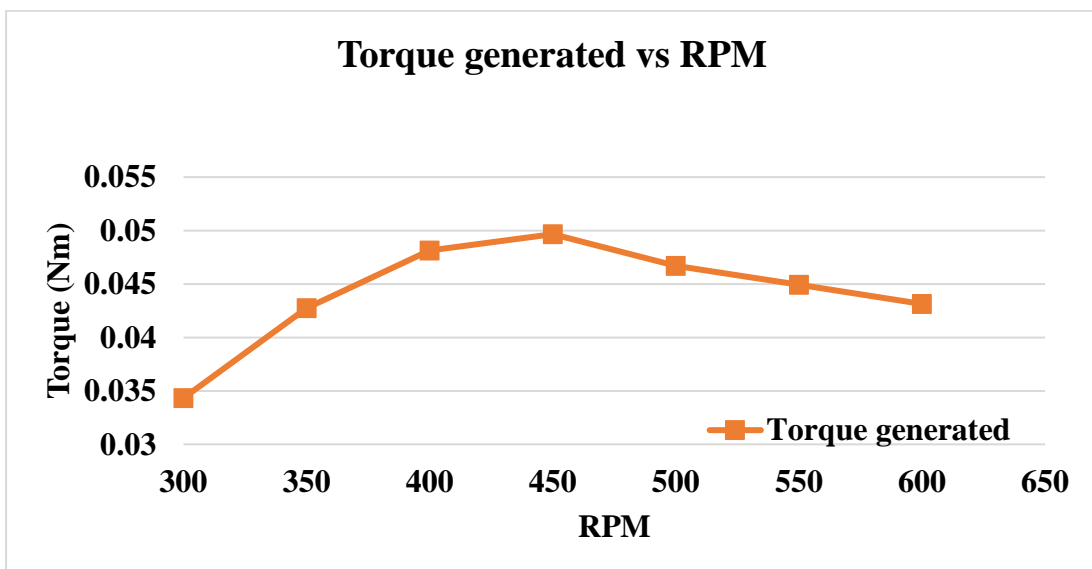
Figure 4.4: Torque vs rotational speed of blade with aspect ratio 1 at 5.8346 m/s

56

d) Static pressure and velocity distribution on rotor blade with aspect ratio 1

The figure below shows the pressure contour of the rotor blade with aspect ratio 1 at a rotational speed of 31.41 rad/s for wind speed 5 m/s. The figure below shows that minimum and maximum static pressure at 5 m/s are -214.2 pa and 29.49 pa respectively.
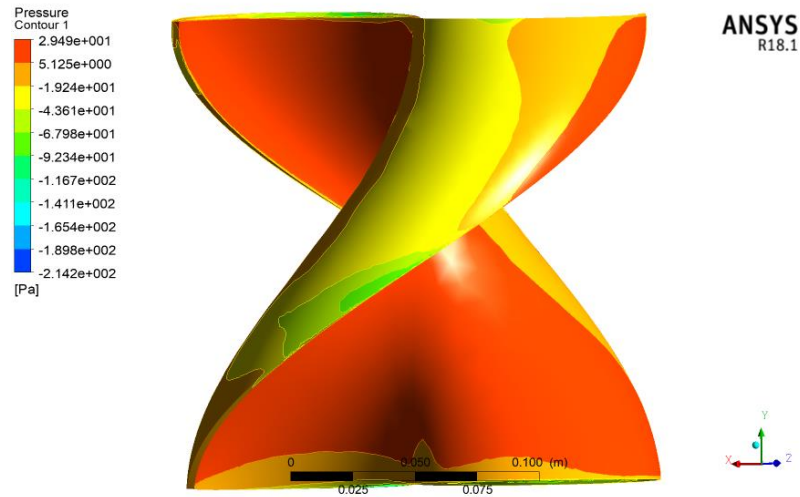
Figure 4.5: Static pressure contours of rotor with aspect ratio 1

Due to the helical shape of the proposed rotor, there is a significant pressure difference between the front and rear side of the helical shaped rotor which can generate the torque.
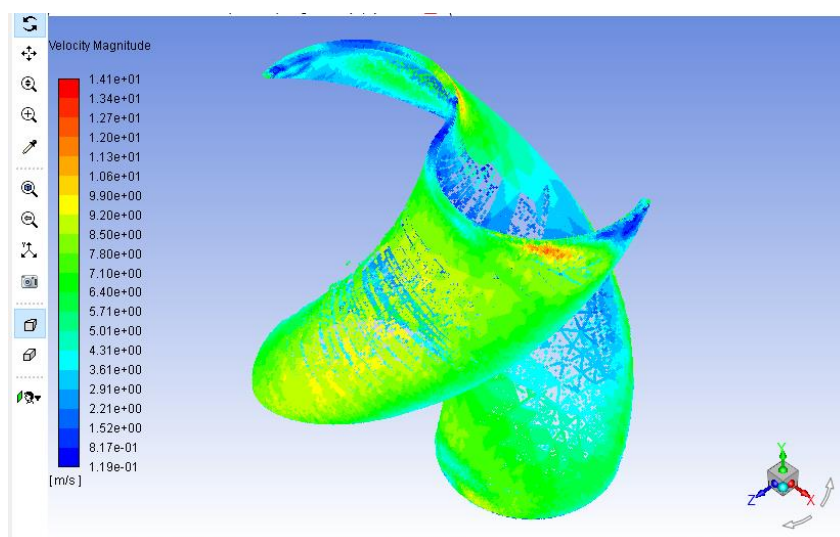
Figure 4.6: Velocity contours of the rotor with aspect ratio 1

The figure above shows the velocity contour of the rotor blade with aspect ratio 1 at a rotational speed of 31.41 rad/s for wind speed 5 m/s. The velocity contours give the information that the maximum velocity was available at the tip of the blade with a value of 14.1 m/s and minimum at the shaft line of the rotor.

4.2 Result via Wind Tunnel Testing

Different results are analysed by the help of an experiment that was performed at the lab of Kathmandu University. They are as follows:

a) Comparison between velocity and rpm of fabricated modal
b) Comparison of C_p of fabricated VAHWT generated via CFD and experiment
c) Comparison of torque generated via CFD and experiment
d) Comparison of power generated via CFD and experiment
e) Result from uncertainty analysis

Explanation of these outcomes are as follows:

a) Comparison between velocity and rpm of fabricated modal

The rotational speed of the highly efficient rotor blade at different inlet wind speed was measured. To be more precise and accurate, 9 experiments with 20 sample readings were taken and their average was taken for further calculations. The graph shows the relation between the inlet velocity and rotational speed of the fabricated model.
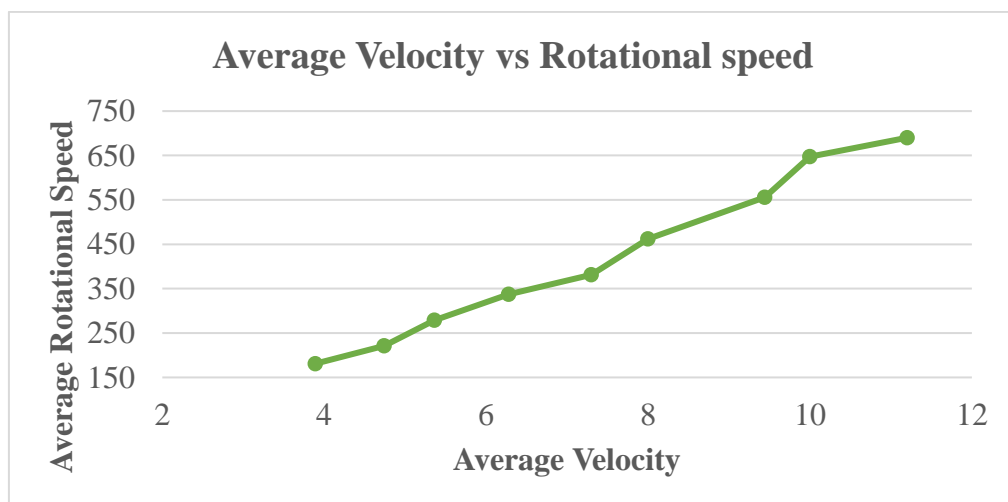
Figure 4.7: Average speed vs rotational speed graph

58

The graph shows the information between the rotational speed of the rotor and wind tunnel inlet velocity. The slope of the curve generated seems increasing positively which signified the increase of rotational speed with an increase in average wind speed. The line between average rotational speed and inlet velocity seems almost straight and linear. This shows there is a linear relationship between the wind speed and the rotational speed of the rotor. Thus, the data generated can be considered quite satisfactory.
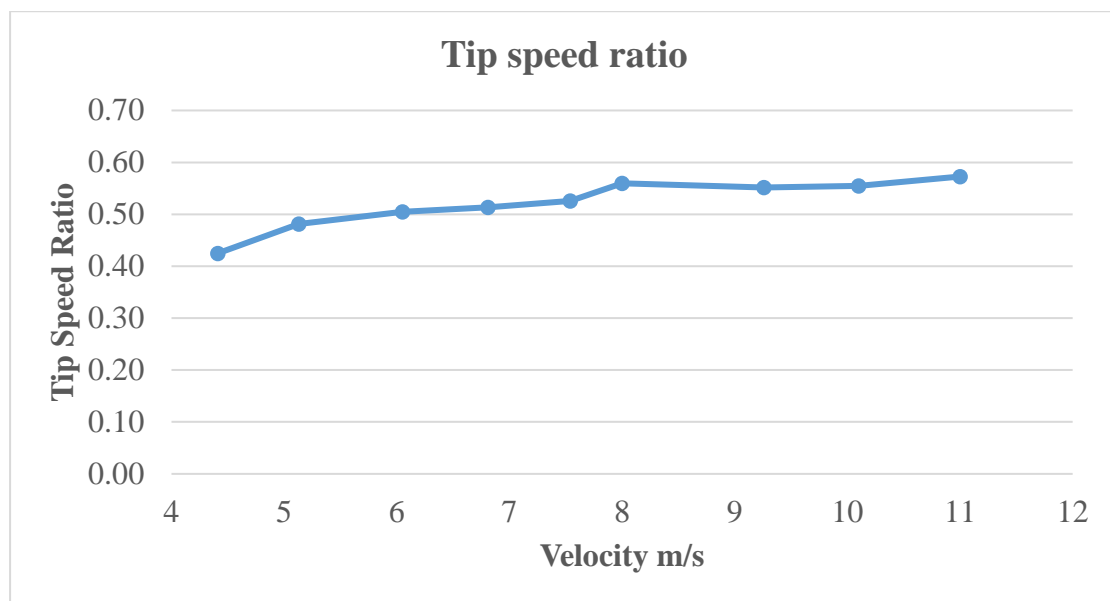
Figure 4.8: Tip speed ration with respect to inlet velocity of blade with aspect ratio 1

The figure gives information about varying tip speed ratio with respect to the inlet velocity of the wind. It shows that the more stable tip speed ratio is available between 5.36 m/s to 7.3 m/s inlet wind speed and the wind turbine has an optimal tip speed ratio at 10 m/s with a value of 0.63.

b) **Comparison of C_p of fabricated VAHWT generated via CFD and experiment**

The slope of C_p (CFD) and C_p (experiment) is presented below and the Coefficient of performance gap between these two curves seems very small at first and fluctuated to 8m/s speed and then remains constant. Thus, validating the data generated via CFD and measured via experimental test and the gap between this graph is due to errors in fabrication and experiment. The errors on fabrication were due to using non-standard coupling between the rotor shaft and generator, using a rapid prototyping machine for

the fabrication of the rotor caused less smooth surface and small bearing size losses. And the errors in the experiment were due to poor knob adjustment on the wind tunnel potentiometer for varying inlet velocity, electric circuit losses etc.
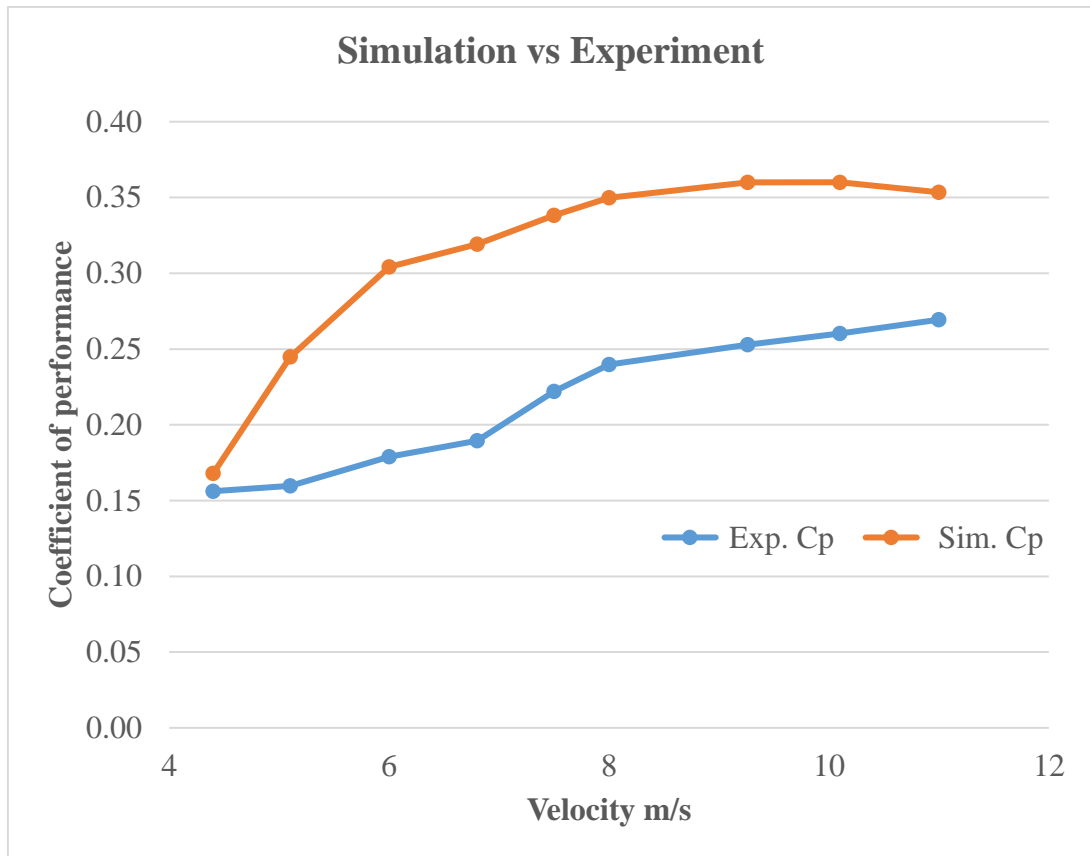
Figure 4.9: Comparison of C_p of fabricated rotor generated via CFD and experiment

From the above graph, it can be concluded that the value of the performance coefficient calculated via experiment ranges from 0.15 to 0.27 while CFD ranges from 0.16 to 0.36 in the velocity range of 4.4 to 11 m/s. The experimental data is less compared to CFD because of mechanical losses. At the low wind speed, the difference between the experiment and simulation performance coefficient was small and the gap fluctuated to 8 m/s and then nearly constant with the difference of 9%. At the low wind speed, the rotational speed of the rotor was less than the maximum possible rotational speed due to several mechanical losses. After the 8 m/s wind speed, the tip speed ratio was stable which can give the constant losses. This gap between the simulation and experiment performance coefficient was due to several mechanical losses under the fabrication and experiment section. The cause of mechanical losses is explained above.

c) Comparison of torque generated via CFD and experiment

The slope of torque (CFD) and torque (experiment) is presented below and the slope of both curves seems almost the same thus validating the data generated via CFD and measured via experimental test.
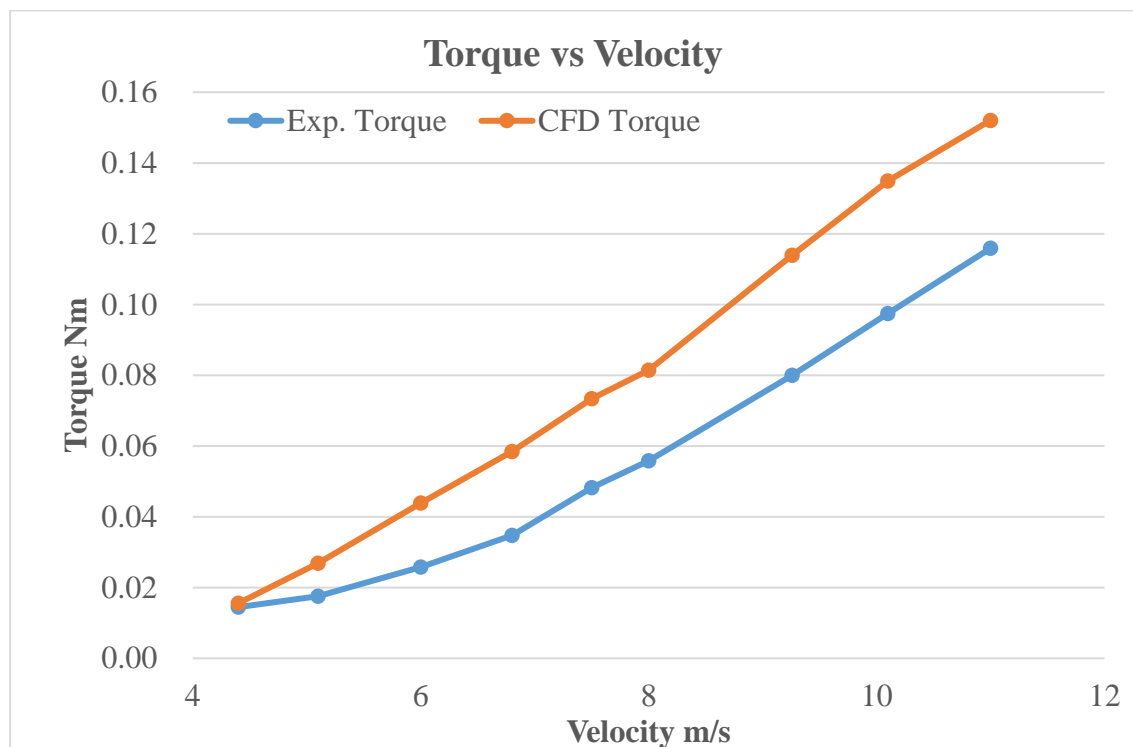
Figure 4.10: Torque comparison of fabricated rotor generated via CFD and experiment

It can be observed that the value of the torque produced experimentally ranges from 0.01476 to 0.11626 while produced via CFD ranges from 0.01557 to 0.15203. The gap between the two values was mainly due to the eccentric coupling between shaft and generator and poor knob adjustment potentiometer on the wind tunnel. However, the slope of both curves was similar which signifies the uniformity relationship between torque generation and inlet velocity on both CFD and experimental methods.

d) Comparison of power generated via CFD and experiment

The graph between experimental and theoretical power is presented below and the power gap between these two curves is very less at first and increased later.
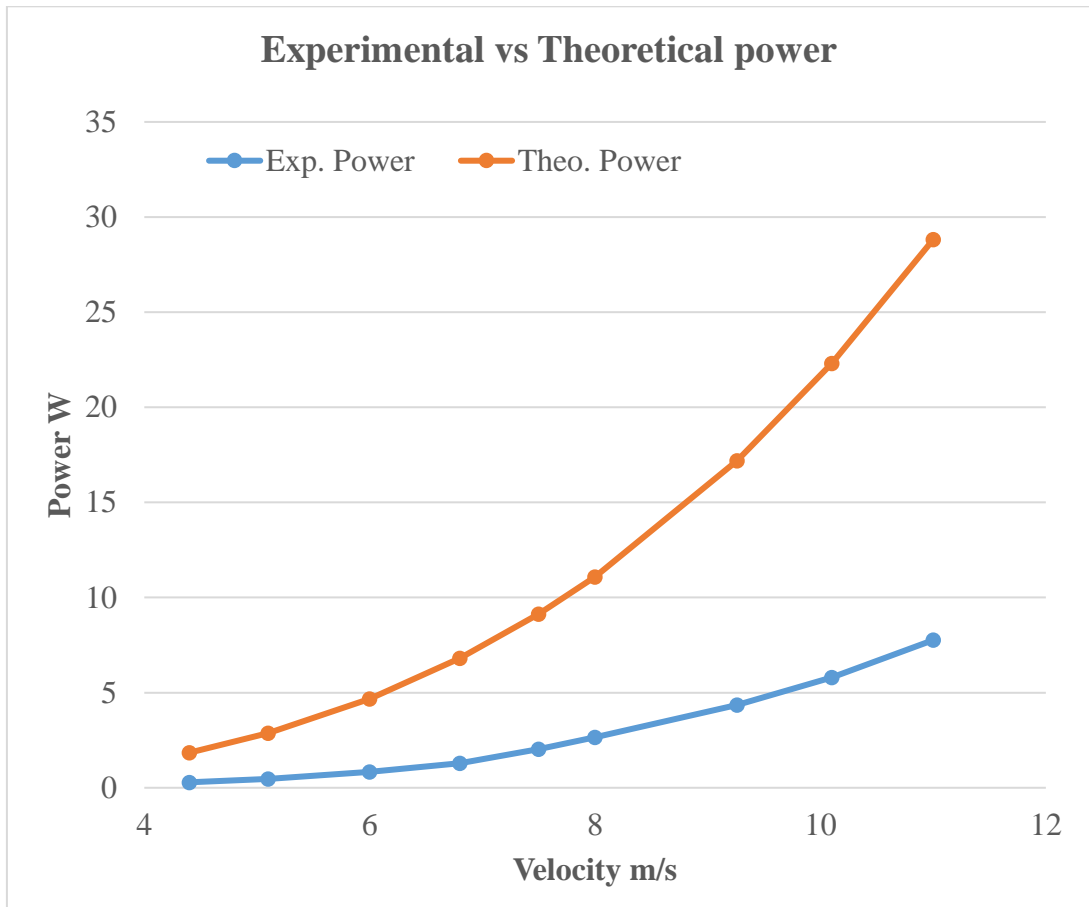
Figure 4.11: Comparison between the power generated via the experimental and theoretical method

It can be noticed that the power produced experimentally increased linearly ranges from 0.294 to 7.788 watts while the theoretical power increased rapidly from 1.856 to 28.813 watts. The theoretical power is exponentially dependent on the wind inlet velocity. Therefore, while increasing the inlet velocity, there is exponential increase in the theoretical power as shown in the curve above. But according to the Betz limit, only 40% of the theoretical wind power transmit to the experimental power. Due to some mechanical losses under the experimental section and Betz limit, the difference between theoretical and experimental power occurred. However, both of the curves identify that they are increased uniformly with respect to wind speed.

The graph below gives information about the curve between numerical modeling and theoretical power. The simulation power increased linearly from 0.310 to 10.183 watts where the theoretical power added rapidly. The gap between these powers is due to the Betz limit and simulation considerations. The theoretical power curve goes on

exponential rate and the Betz limit gives the information that only 59.3 % of wind energy is used for rotation of the turbine. There were no mechanical losses while using simulation which ultimately gives the gap between theoretical and simulation power generation.
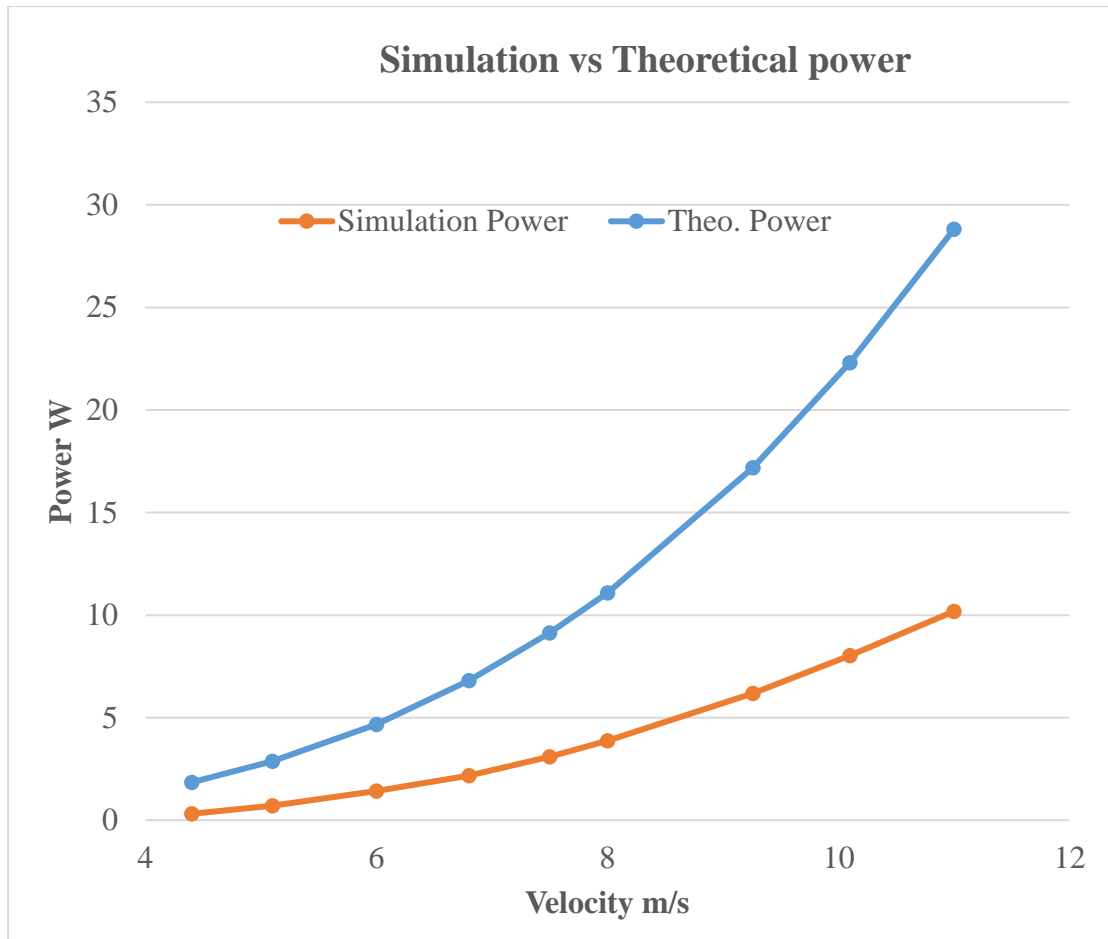
Figure 4.12: Comparison between the power generated via Numerical modeling and theoretical method

The curve produced by the experimental and simulation power is presented below and the slope of both curves seems almost same thus validating the data generated via CFD and measured via experimental test. It can be observed the value of the power produced experimentally ranges from 0.294 to 7.788 while produced via CFD ranges from 0.310 to 10.183. The gap between two values is due to mechanical losses as explained above. However, the slope of both curves is identical which signifies there is a uniform increase of power with respect to wind velocity in both the experimental and CFD approach.
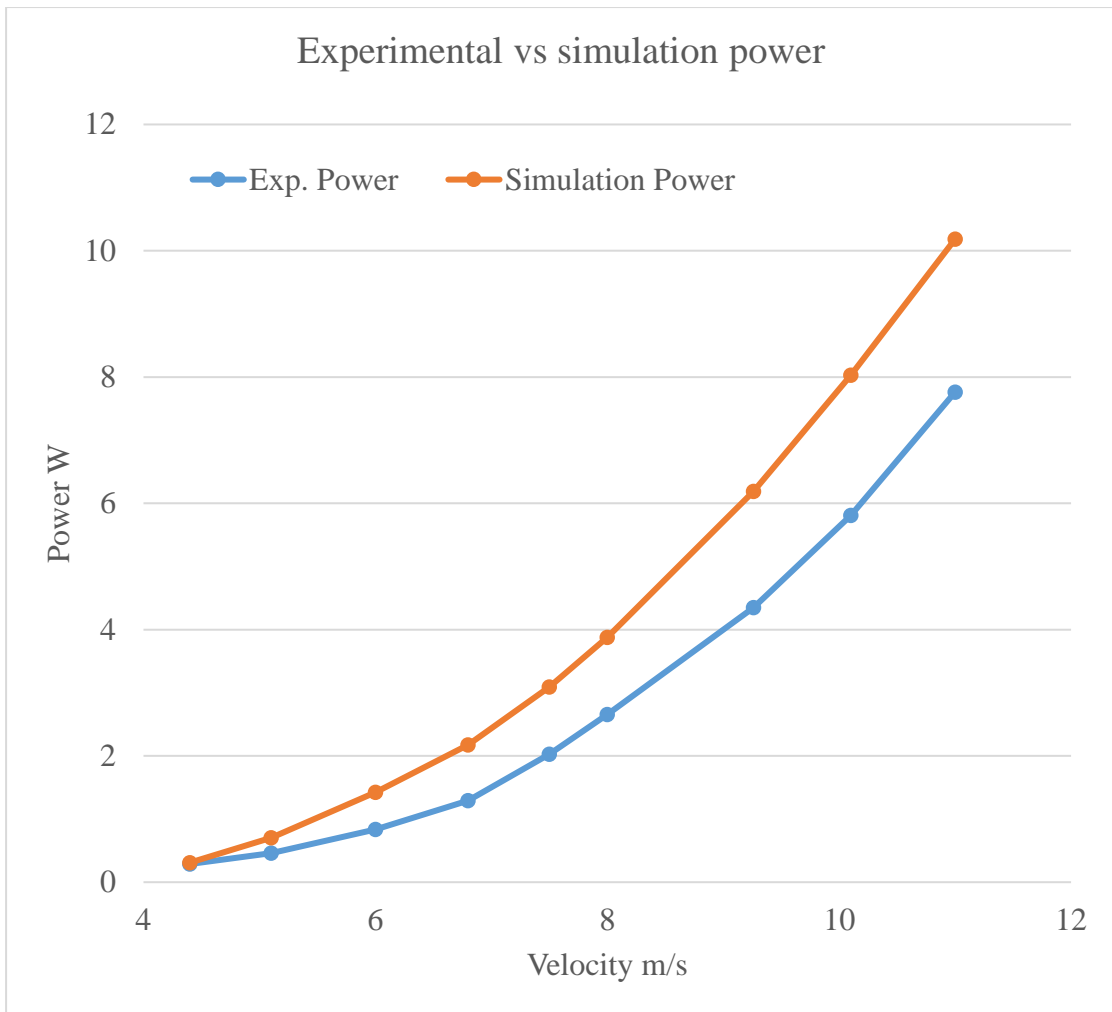
Figure 4.13: Comparison between the power generated via experimental and numerical modeling method

e) Result from uncertainty analysis

The uncertainty analysis was carried out to know the percentage of the error caused by the measurement instrument. The below graph gives information about the nature of error with respect to the power output from the generator. While increasing the power output, the error percentage decrease due to constant electric circuit losses. At the low initial velocity, there was low power output but the electric circuit losses may occur constantly. Therefore, the percentage error is high at low power output. Similarly, the output power was 7.76 W at the velocity of 11 m/s but the electric circuit losses may remain constant. The percentage error is inversely proportionate to the power output. So, while increasing the power output, the percentage error was decreasing in trend due to constant electric circuit losses.
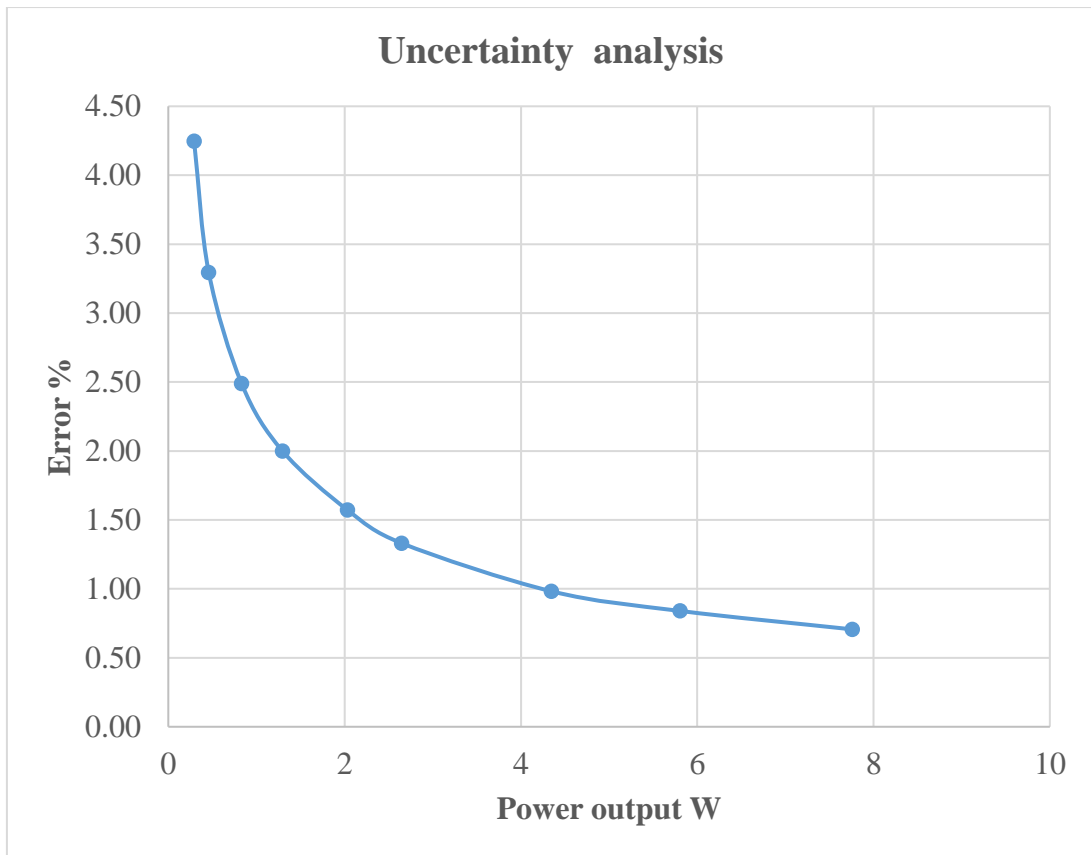
Figure 4.14: Error percentage calculation at different power measurement

4.3 Result via impact wind energy analysis at Sallaghari

The average vehicle speed at Sallaghari was recorded with respect to their different modes with the help of a questionnaire. It shows that the speed of the vehicles decreased from light to heavy vehicles or from two-wheeler to ten-wheeler vehicles i.e. The 2-wheeler vehicles have the highest average speed than other modes of vehicles. The average speed of the vehicles among all modes was 57 Km/hr.
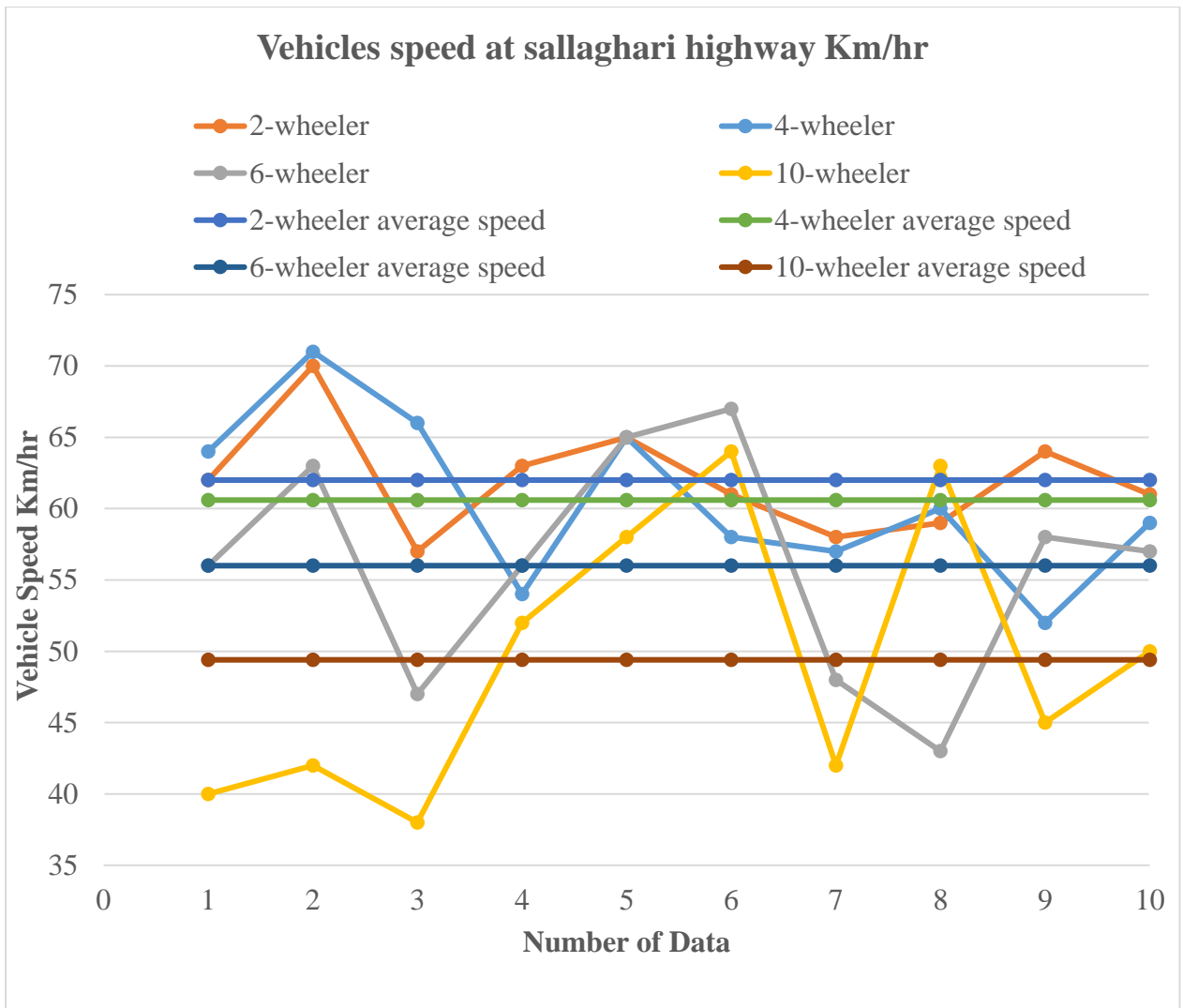
Figure 4.15: Average speed of the vehicles at Sallaghari

The experiment data carried out helps to analyze the pattern of impact wind energy available on highways. For this, the velocity of impact wind energy was carried out to predict the maximum velocity of impact wind energy available at different times throughout the day which is shown in the figure below.
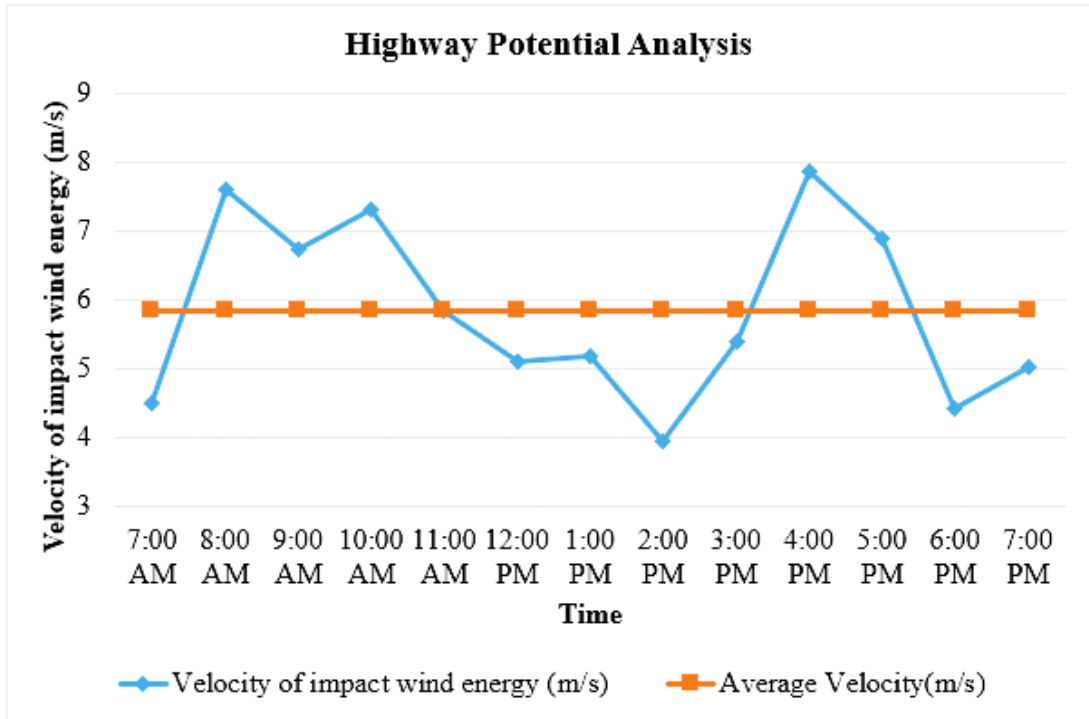
Figure 4.16: Impact wind energy available at Sallaghari highway with respect to time

The experiment data carried out at Sallaghari highway shows that the maximum impact wind speed of 7.61 and 7.89 m/s were available at 8 am and 4 pm respectively due to heavy-duty vehicles and more traffic in highways. Also, it was noticed that the lowest impact wind energy is around 3.95 m/s at 2 pm due to less vehicle flow and the average velocity of wind is around 5.8346 m/s. The maximum power output of 3.46 watts was available at 4 pm with the proposed model rotational speed of 446 rpm and the average power output of 1.53 watts was available at Sallaghari.

CHAPTER FIVE: CONCLUSIONS AND RECOMMENDATIONS

5.1 Conclusions

The major findings of the thesis work can be summarized as below:

- The coefficient of performance at different aspect ratios was calculated by the Computational fluid dynamic approach and the maximum coefficient of performance of 0.3927 is found on the rotor with aspect ratio 1. Thus, the turbine with aspect ratio 1 is considered to be the most economical turbine based on power generation as well as its efficiency.

- Experimentally, the fabricated rotor has an efficiency of 26.93% which is nearly 9% less than CFD analysis.

- The speed of the vehicles decreased from two-wheeler to ten-wheeler vehicles and the average speed of the vehicles among all modes was 57 Km/hr. Also, the velocity of impact wind energy was around 7.86 m/s as highest at 4 pm which can generate the power of about 3.46 watts at 446 rpm.

5.2 Recommendations

The detailed study carried out during research work has illustrated that VAHWT has a lot of scopes. Thus, detailed research can still be carried out to make it more economical and reliable in the field of wind energy. There is a lot of room for further future works as mentioned below. The recommendations for making the VAHWT more efficient and reliable for commercial production are as follows:

- The angle of curvature of the rotor blade can be varied and its effect on performance can be analyzed by both the CFD approach and experimental setup.

- The use of other materials like Aluminum alloy for the fabrication of blade instead of Plastic material can yield better results due to low weight and compactness. This can be further researched and studied.

- There was a high fluctuation in the flow of wind speed of the wind turbine testing rig. Thus, the use of a digitally controlled speed knob for varying wind speed and pre-installing tools like anemometer within the test rig can help in getting more accurate results.

- The design can be further modified by choosing a better method for fabrication like casting, using standard coupling between generator and rotor shaft, reducing the losses of bearing etc. can make it more efficient and reliable.

- The use of a microcontroller for measurement of impact wind energy throughout the day can help in getting better and efficient results.

- The use of torque sensor for torque measurement instead of calculation of torque in terms of power and rotational speed can give better and accurate result.

REFERENCES

AEOLOS Wind Turbine. (2015, August 24). Retrieved March 13, 2020, from http://www.windturbinestar.com/300w-vertical-wind-turbine

Affordable wind turbines. (2015). Retrieved March 25, 2020, from https://www.affordablewindturbines.org/

Beri, H., & Yao, Y. (2011). Effect of Camber Airfoil on Self Starting of Vertical Axis Wind Turbine. *Journal of Environmental Science and Technology*, 302-312. DOI:10.3923/jest.2011.302.312

Briefs, T. (2011). *Create the Future*. Retrieved April 02, 2020, from https://contest.techbriefs.com/2011/entries/sustainable-technologies/1754

Cheng, Q. a. (2017). Aerodynamic analysis of a helical vertical axis wind turbine. *Energies, 10*, 575. DOI:10.3390/en10040575

Deb, B. a. (2014). Experimental analysis of a 20 twist helical savonius rotor at different overlap conditions. *Applied Mechanics and Materials, 592*, 1060--1064. DOI:AMM.592-594.1060

Eldridge, F. R. (1975). *Wind machines* (Vol. 75). The Foundation. Retrieved March 25, 2020,fromhttps://books.google.com.np/books/about/Wind_machines.html?id=tBLcHf OgVo0C&redir_esc=y

GWEC. (2019). *Global Wind Report.* Global Wind energy council. Retrieved July 10, 2020, from https://gwec.net/global-wind-report-2019/

Hockenos, P. (2019, April 2). Germany's Winds of Change. *Coastal science and societies*. Retrieved May 15, 2020, from https://www.hakaimagazine.com/features/germanys-winds-of-change/

Hussen, M. S. (September 2015). Design and Analysis of Vertical Axis Wind Turbine Rotors. *International Journal on Recent Technologies in Mechanical and Electrical Engineering (IJRMEE)*. DOI: 10.1016/j.oceaneng.2012.09.007

Jeon, K. S.-K.-W. (2015). Effects of end plates with various shapes and sizes on helical Savonius wind turbines. *Renewable energy, 79*, 167--176. DOI:10.1016/j.renene.2014.11.035

LernMech. (2015, June 3). Retrieved March 20, 2020, from FABRICATION OF VERTICAL AXIS WIND TURBINE: https://learnmech.com/fabrication-of-vertical-axis-wind/

Marmutova, S. (2016). *The improved Savonius wind turbine captures wind in the cities.* Vaasan Yliopisto. Retrieved February 27, 2020, from https://www.sciencedaily.com/releases/2016/05/160520101617.htm

Md Aminul Hassan, D. C. (2014). Analysis of Highway Wind Energy Potential. *International Journal of Engineering Research & Technology (IJERT), 3*, 1496--1498. Retrieved from https://www.ijert.org/research/analysis-of-highway-wind-energy-potential-IJERTV3IS041653.pdf

NEA. (2019). *Nepal Electricity Authority Annual Report 2076.* Kathmandu. Retrieved August 4, 2020, from file:///C:/Users/Pradeep/Downloads/annual_report_2076.pdf

Oy Windside Production Ltd. (2015). *WINDSIDE*. Retrieved February 23, 2020, from https://www.windside.com/products/ws-0_15

Pokharel, S. (2001). Hydropower for Energy in Nepal. *Researchgate*, 4-9. DOI:10.1659/0276-4741(2001)021[0004:HFEIN]2.0.CO;2

qureshi, y. (2018, june 13). *Prezi*. Retrieved from Design analysis and fabrication of spiral and helical vertical axis wind turbine: https://prezi.com/avlnhi9osk-t/design-analysis-and-fabrication-of-spiral-and-helical-vertical-axis-wind-turbine/

Ragheb, M. (2015). *VERTICAL AXIS WIND TURBINES*. Mragheb. Retrieved from https://d1wqtxts1xzle7.cloudfront.net/40749609/Vertical_Axis_Wind_Turbines.pdf

Rai, S. (2019). *Introduction to RE Mini Grid Projects.* Alternative Energy Promotion Center Nepal. Retrieved from https://energypedia.info/images/6/6a/Session_0_Introduction_AEPC_Mr._Rai_090419.pdf

Reza, A. a. (2015). Construction of a helical vertical axis wind turbine for electricity supply. *Computer-aided Design and Applications*, 9--12. DOI:10.1080/16864360.2015.1077069

S. Brusca, R. L. (2014). Design of a vertical-axis wind turbine: how the aspect ratio affects the turbine's performance. *International Journal of Energy Environment Engineering*. DOI:10.1007/s40095-014-0129-x

S.S.Suprajha, & K.Vijayan. (May 2016). Design and Analysis of Helical Blade Wind Turbine. *International Journal of Innovative Research in Science,Engineering and Technology*. DOI:10.15680/IJIRSET.2016.0505224

Saad, A. S.-A. (2017). Performance analysis of a helical Savonius wind turbine with modified rotor. *International Conference on Aerospace Sciences and Aviation Technology. 17*, pp. 1--14. The Military Technical College. DOI:10.21608/asat.2017.22459

TECHCARBON. (2017). *Helix Wind Turbine,Wind of Change*. Retrieved June 10, 2020, from http://www.wind-of-change.org/

Tjiu, W., Marnoto, T., Sohif, M., Ruslan, M., & Sopian, K. (2015). Darrieus vertical axis wind turbine for power generation I: Assessment of Darrieus VAWT configurations. *Researchgate*, 50-67. DOI:10.1016/j.renene.2014.09.038

Upreti, B., & Shakya, A. (2009). *WIND ENERGY POTENTIAL ASSESSMENT IN NEPAL.* APECWW. DOI:10.3126/njst.v11i0.4139

Vinit V. Bidi, D. M. (2017). Highway Power Generation Using Low Cost Vertical Axis Wind Turbine. *International Journal of Engineering Science and Computing (IJESC)*.

Zhou, A. (2017). *NEPAL ENERGY SECTOR ASSESSMENT, STRATEGY, AND ROAD MAP.* ADB. DOI:10.22617/TCS178936-2

PUBLICATION

Bartaula, P., & Shakya, S. R. (2020). *Design and Numerical Modelling of Vertical Axis Helical Wind Turbine for Highway Application*. Kathmandu: IOE Graduate Conference.

Appendix A: Wind tunnel testing data

Table A.1: Wind tunnel Experimental data of the proposed model while testing

S.N.	Experiment 1		Experiment 2		Experiment 3		Experiment 4		Experiment 5		Experiment 6		Experiment 7		Experiment 8		Experiment 9	
	Velocity	Rpm	Velocity	Rpm	Velocity	Rpm	Velocity	Rpm	Velocity	Rpm	Velocity	Rpm	Velocity	Rpm	Velocity	Rpm	Velocity	Rpm
1	3.65	168	4.303	206.5	5.3	279	6.22	333	7.31	380.5	8.49	476.4	9.26	546.6	10.4	671.6	11.1	695.4
2	3.693	170	4.7	219	4.917	251	5.925	315.6	7.47	387.2	8.22	466.8	9.55	575.6	10.35	660.4	11.2	694.9
3	3.73	156	4.931	241	4.91	258.2	6.2	329.4	7.52	392	8.25	463.5	9.36	556	10.24	653.6	11.1	682.3
4	3.81	166	4.906	234.4	5.015	264.4	6.12	340.5	7.43	382.5	8.2	474	9.452	563.6	10.45	658.3	11.2	684.2
5	3.94	167	4.71	215	4.92	257	6.215	328	7.62	402.5	8.16	469.6	9.747	577.2	10.26	664	11.1	676.9
6	3.785	182	4.692	208.3	5.385	275.4	6.42	346.2	7.581	400.1	8.324	465.1	9.58	563.6	10.42	688	11.1	675.8
7	4.093	197	4.742	220.8	5.8	317	6.12	326.4	7.32	393.6	7.965	450.5	9.72	596.4	10.39	667.4	11.1	679.2
8	3.956	193	4.931	234	5.741	310.4	6.47	350.4	7.501	384.8	8.02	447.7	9.806	594.5	10.31	683.3	11.1	682.6
9	3.938	192	4.837	217.6	5.167	275	6.472	345.2	7.4021	373.7	8.497	477.6	9.65	570.8	10.42	684.7	11.3	692.6
10	3.818	186	4.842	226	4.98	261	6.621	359.6	7.62	410.6	8.1	468.6	9.74	580.5	10.32	667	11.1	688.7
11	3.849	184.5	4.768	228.4	5.135	268.4	6.37	347	7.53	397	8.14	461.6	9.358	545.7	9.5	600.51	11.1	683.7
12	3.875	185.2	4.751	217.5	5.696	278	6.13	319.6	6.95	362.6	7.96	450.4	9.478	559.2	9.6	604.1	11.2	703.8
13	3.793	165.8	4.8	211	5.122	270	6.125	325.6	7.214	369.9	8.34	465.7	9.36	548.2	9.5	598.6	11.2	689.8
14	3.598	195.7	4.575	206.2	5.68	284.5	6.005	320	6.826	358.4	8.48	467.2	9.7	587.5	10.3	670.6	11.1	694.2
15	3.709	174.2	4.565	214	5.718	307.8	6.501	350.2	7.035	371.1	8.31	469.7	9.54	568.2	9.75	623.6	11.3	705.6
16	4.22	189.2	4.691	221	5.51	269	6.46	344.2	6.825	360.2	8.43	489.9	8.9	504	9.68	602.5	11.39	698.6
17	4.11	190	4.567	217.5	5.731	302.5	6.625	351.2	7.054	371.5	7.6	417.3	9.26	533.4	9.85	629	11.209	686.5
18	4.263	200.2	4.805	227.2	5.103	268.5	5.915	320	7.2	381.2	7.902	443.8	9.154	517.1	9.96	639	11.51	708.2
19	3.986	191.2	4.807	225.4	5.642	284.4	6.125	335.4	7.35	372.5	8.025	449.2	9.01	508	10.09	638.6	11.3	692.6
20	4.081	166	4.88	237.8	5.731	296.4	6.75	355	7.35	375.6	4.45	472.2	9.25	514.8	9.94	640.2	11.17	684.6
Average	3.89485	180.95	4.74015	221.43	5.36015	278.895	6.28945	337.125	7.30541	381.375	7.99315	462.34	9.44375	555.545	10.0865	647.251	11.194	690.01
Max	4.263	200.2	4.931	241	5.8	317	6.75	359.6	7.62	410.6	8.497	489.9	9.806	596.4	10.45	688	11.51	708.2
Min	3.598	156	4.303	206.2	4.91	251	5.915	315.6	6.825	358.4	4.45	417.3	8.9	504	9.5	598.6	11.1	675.8

Appendix B: Highway potential data

Table B.1: Available impact wind energy recorded at sallaghari highway

Sallaghari highway impact wind speed record at the level of 1.5m height (March 2020)												
	7:00 AM	**8:00 AM**	**9:00 AM**	**10:00 AM**	**11:00 AM**	**12:00 PM**	**1:00 PM**	**2:00 PM**	**3:00 PM**	**4:00 PM**	**5:00 PM**	**6:00 PM**	**7:00 PM**
Impact wind speed m/s	2.83	4.56	3.46	3.17	1.59	2.79	4.91	3.95	3.67	7.86	4.5	3.95	5.02
	3.57	2.85	2.87	3.19	2.22	3.04	4.64	2.11	4.05	5.22	3.98	4.42	4.5
	3.95	3.68	3.07	7.31	5.09	2.87	4.34	3.86	4	3.31	3.48	2.27	3.46
	4.5	3.15	3.62	2.57	4.67	3.84	4.11	3.57	3.94	3.28	3.99	3.69	3.73
	3.07	6.23	6.73	3.36	4.49	3.91	3.7	3.22	3.96	3.56	4.01	3.73	4.24
	3.58	5.99	3.56	4.06	1.81	3.3	3.61	2.18	4.4	3.41	3.63	3.44	4.29
	3.69	4.62	5.09	3.67	5.25	4.06	4.28	2.5	4.93	6.48	6.91	3.14	4.16
	3.38	7.61	5.59	5.45	3.21	4	4.38	3.35	5.4	7.06	3.69	2.94	3.87
	3.32	5.43	6.45	6.32	4.43	5.1	4.5	3.46	4.86	5.99	3.73	3.06	3.68
	3.59	3.99	4.57	3.42	5.84	4.22	5.2	2.96	4.75	4.33	4.55	3.61	3.58
Max Velocity	4.5	7.61	6.73	7.31	5.84	5.1	5.2	3.95	5.4	7.86	6.91	4.42	5.02
Min Velocity	2.83	2.85	2.87	2.57	1.59	2.79	3.61	2.11	3.67	3.28	3.48	2.27	3.46
Average Velocity	3.548	4.811	4.501	4.252	3.86	3.713	4.367	3.116	4.396	5.05	4.247	3.425	4.053

Appendix C: Impact wind potential vs Rotational speed
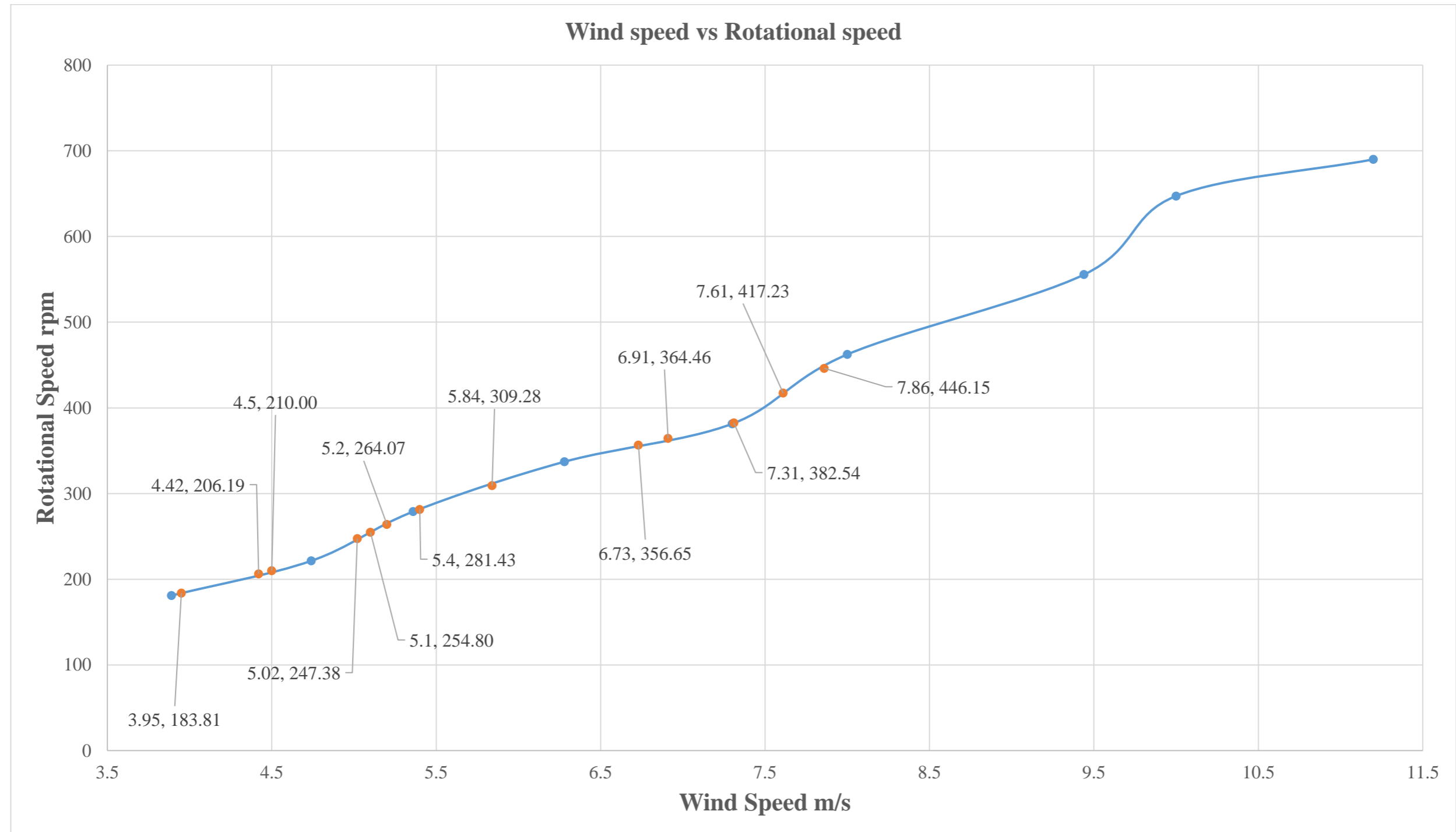
Fig C.1: Calculations of respective rotational speed of the proposed model rotor at sallaghari highway by using interpolation method

Appendix D: Numerical Modelling
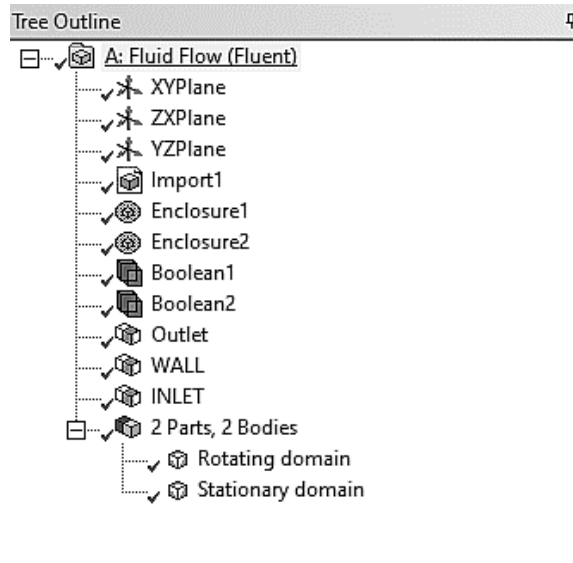
Figure D.1: Tree outline on Design Modeler

Figure D.2: Edge sizing of top semi-circular side of blade

Figure D.3: Edge sizing of edge side helical section of blade
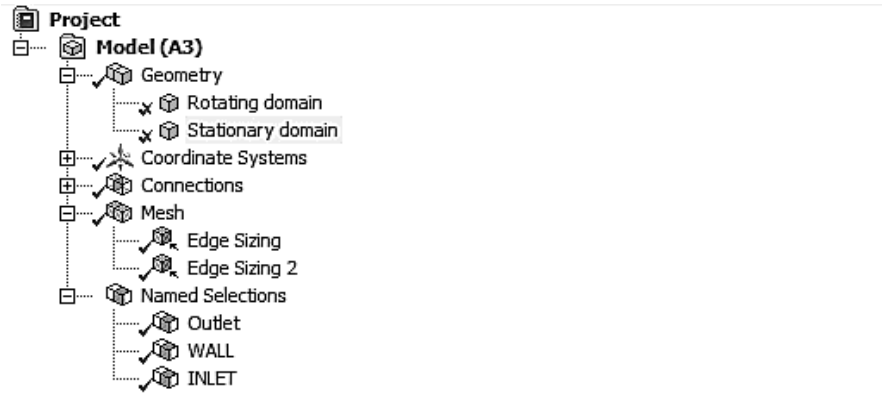
Figure D.4: The outline of the sizing
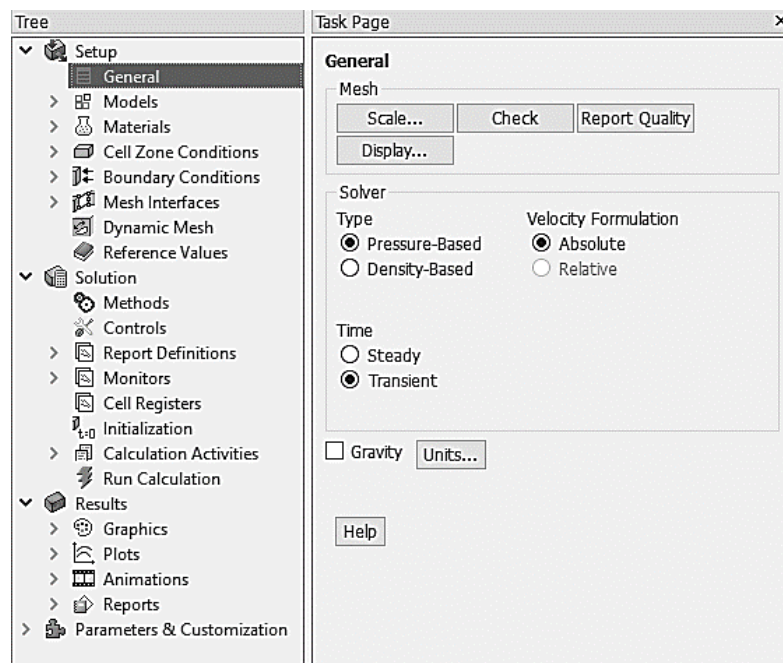
Figure D.5: General setup
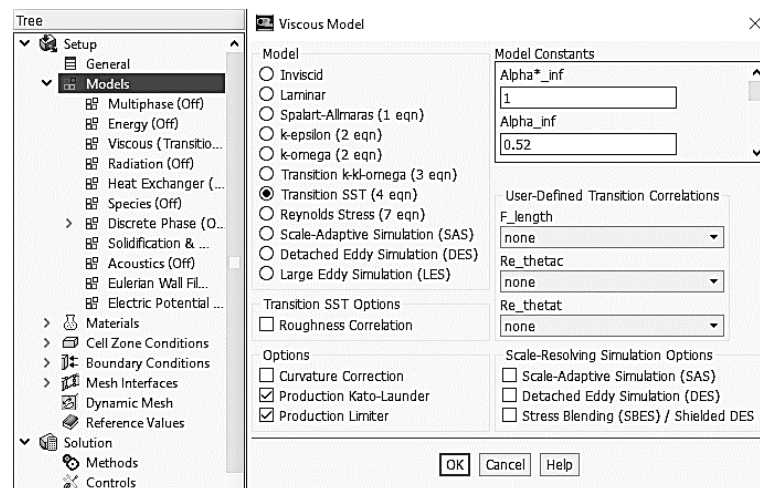
Figure D.6: Selection of viscous model
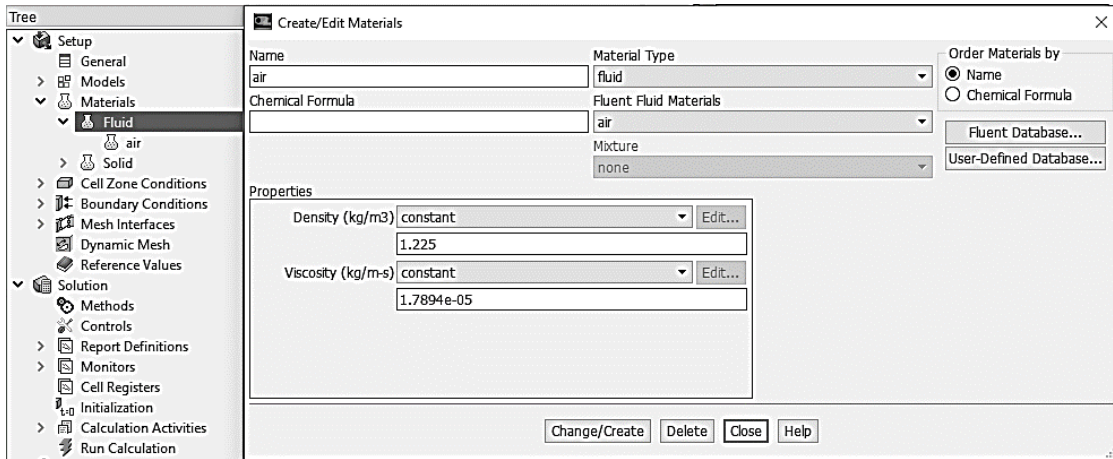
Figure D.7: Fluid material
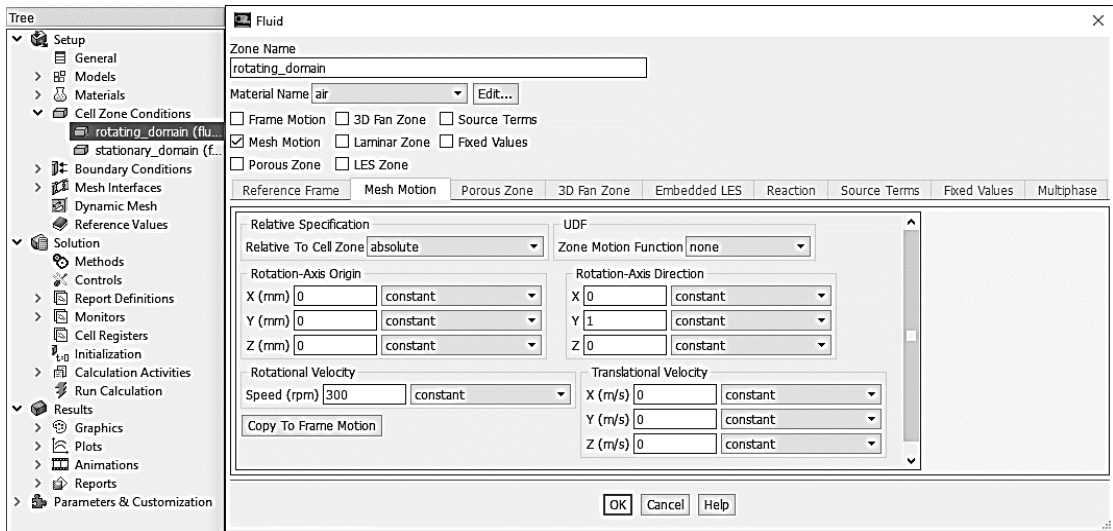
Figure D.8: Cell zone settings
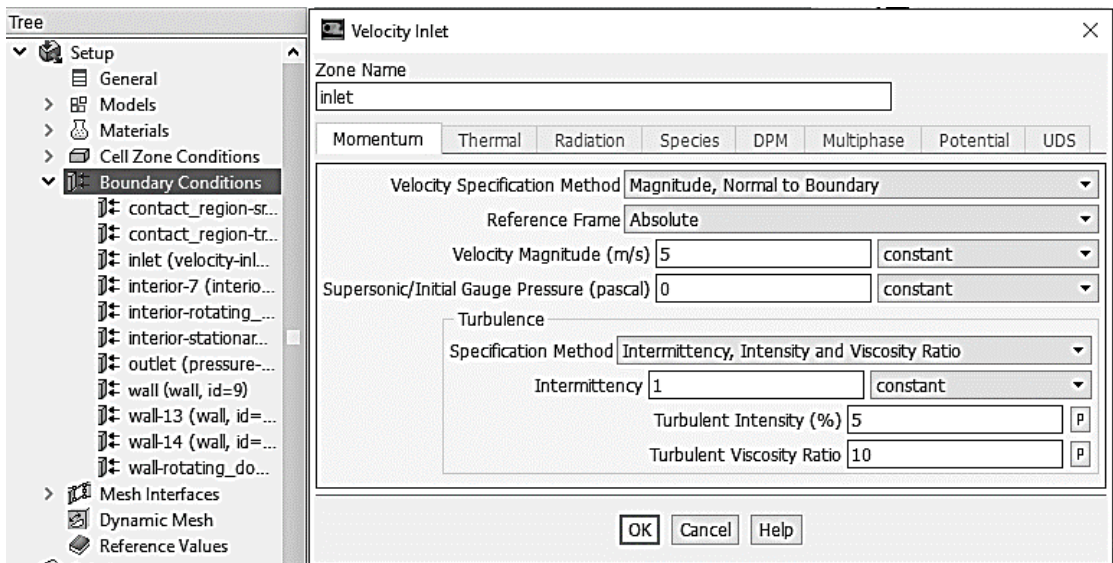
Figure D.9: Inlet boundary condition
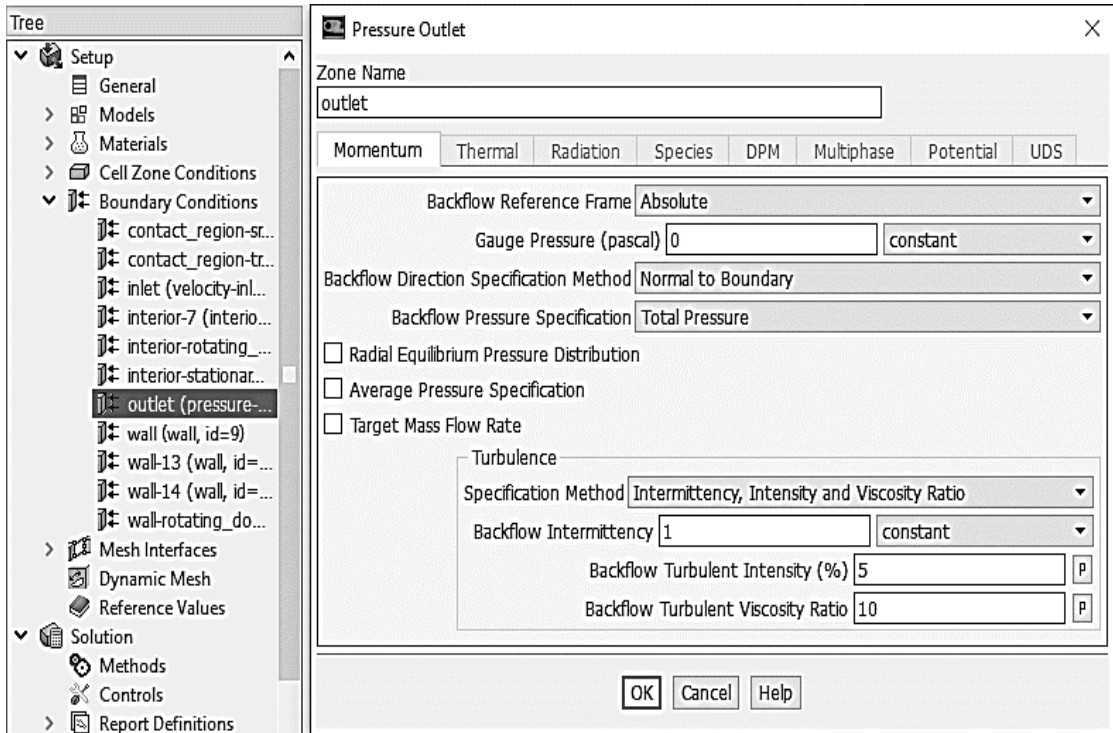
Figure D.10: Outlet boundary condition
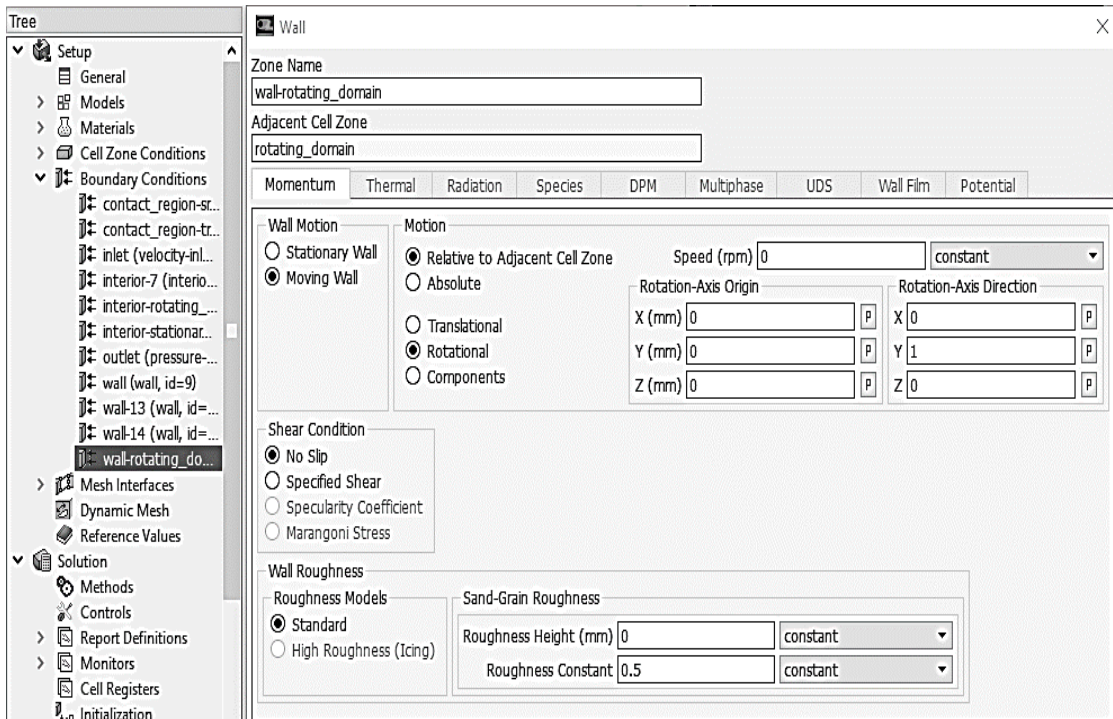
Figure D.11: Rotating domain boundary condition
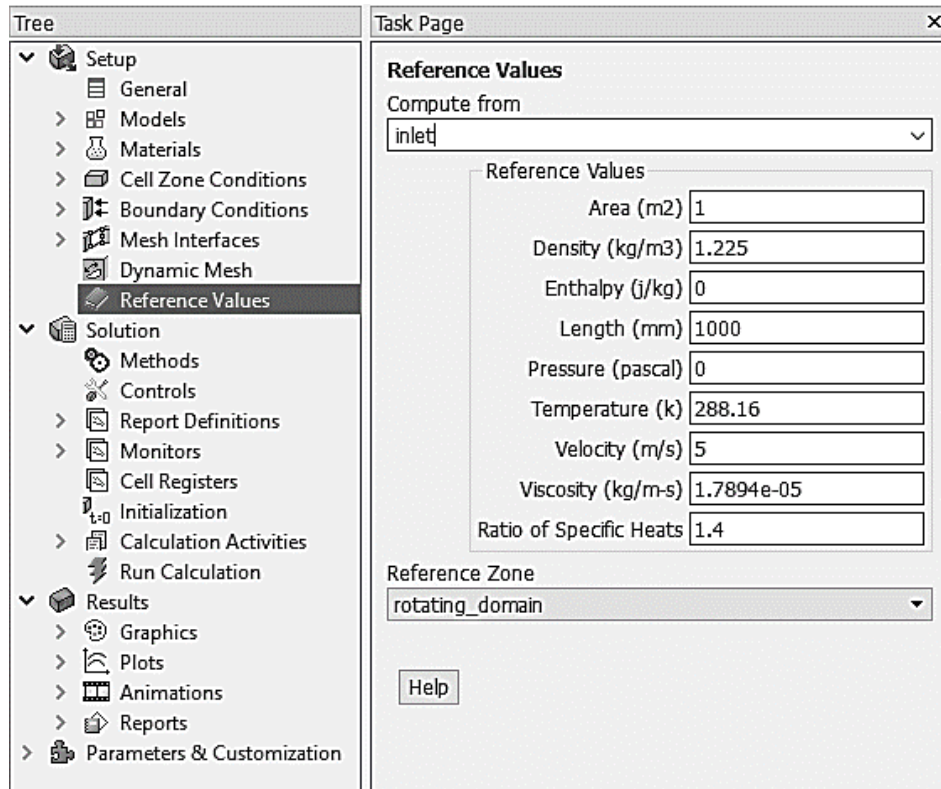
Figure D.12: The default reference values
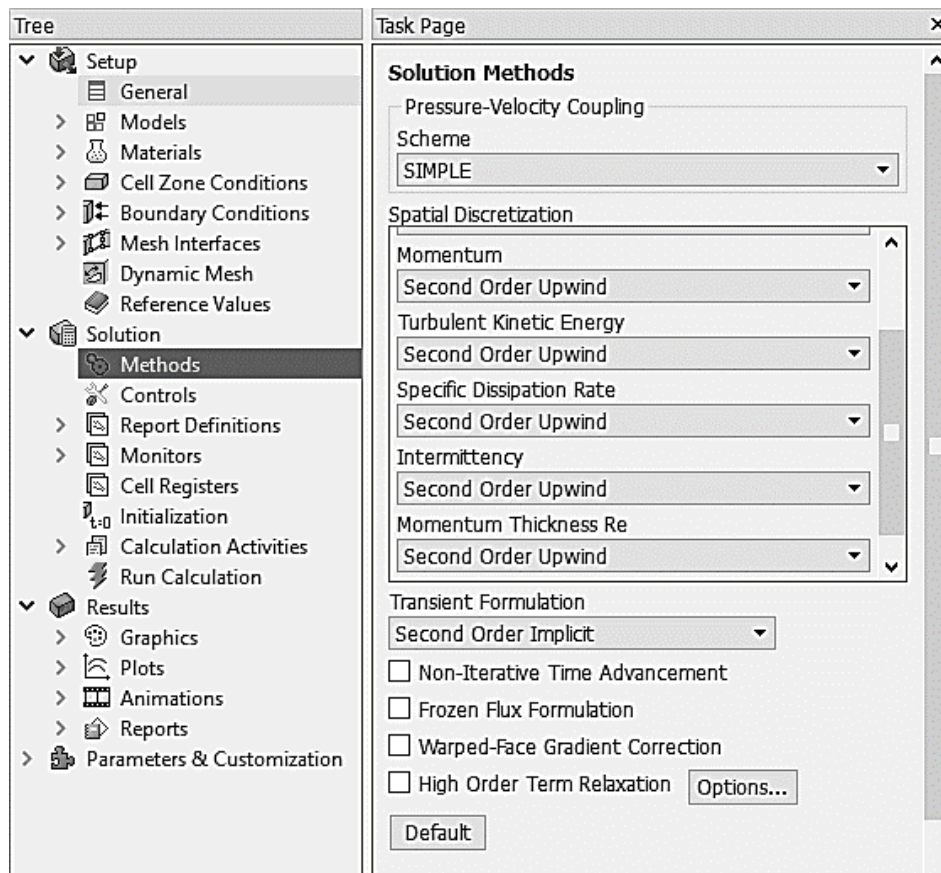
Figure D.13: Solution Methods
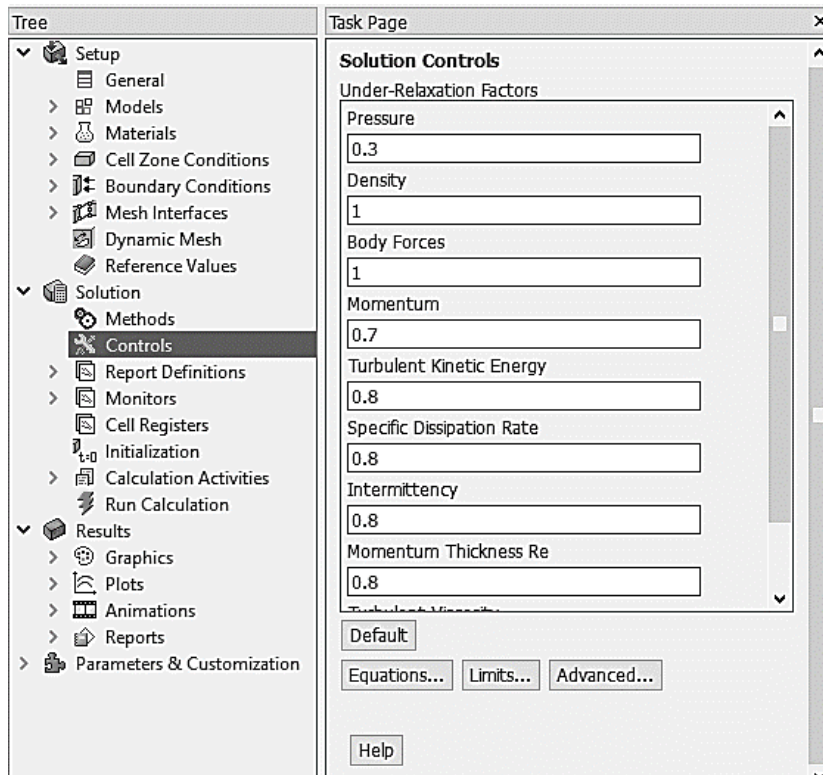
Figure D.14: Solution Controls
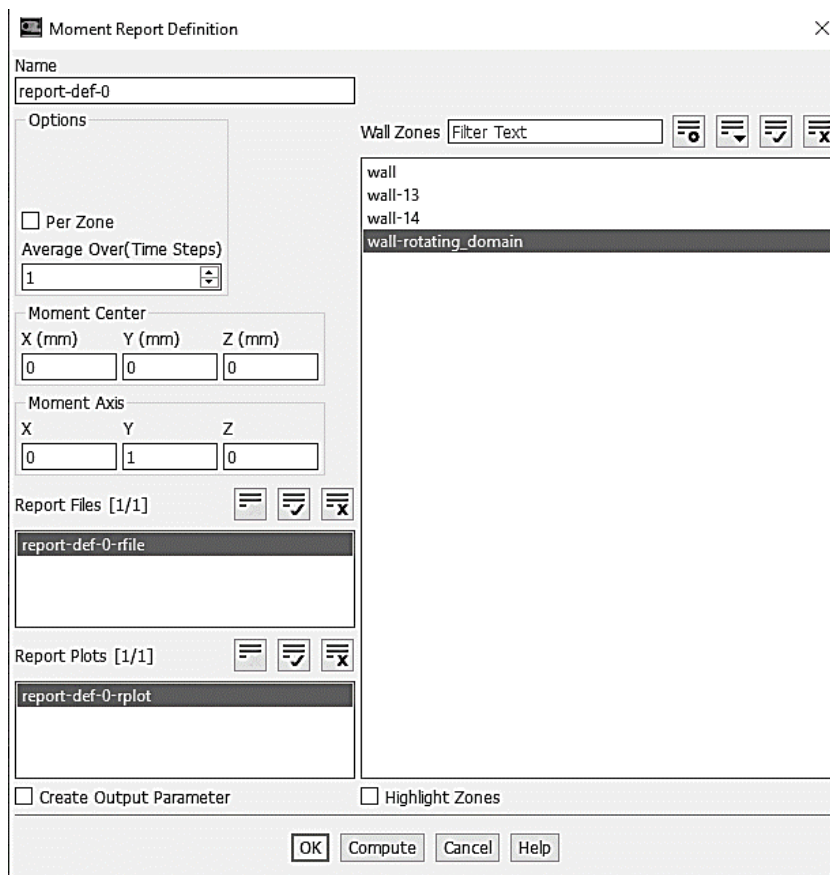
Figure D.15: Selecting axis for moment calculation
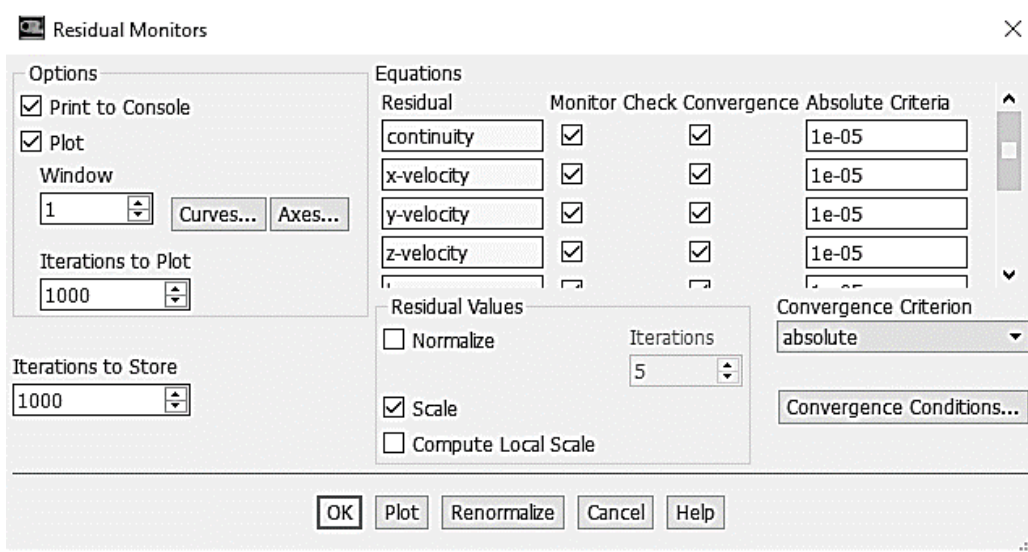
Figure D.16: Residual monitors
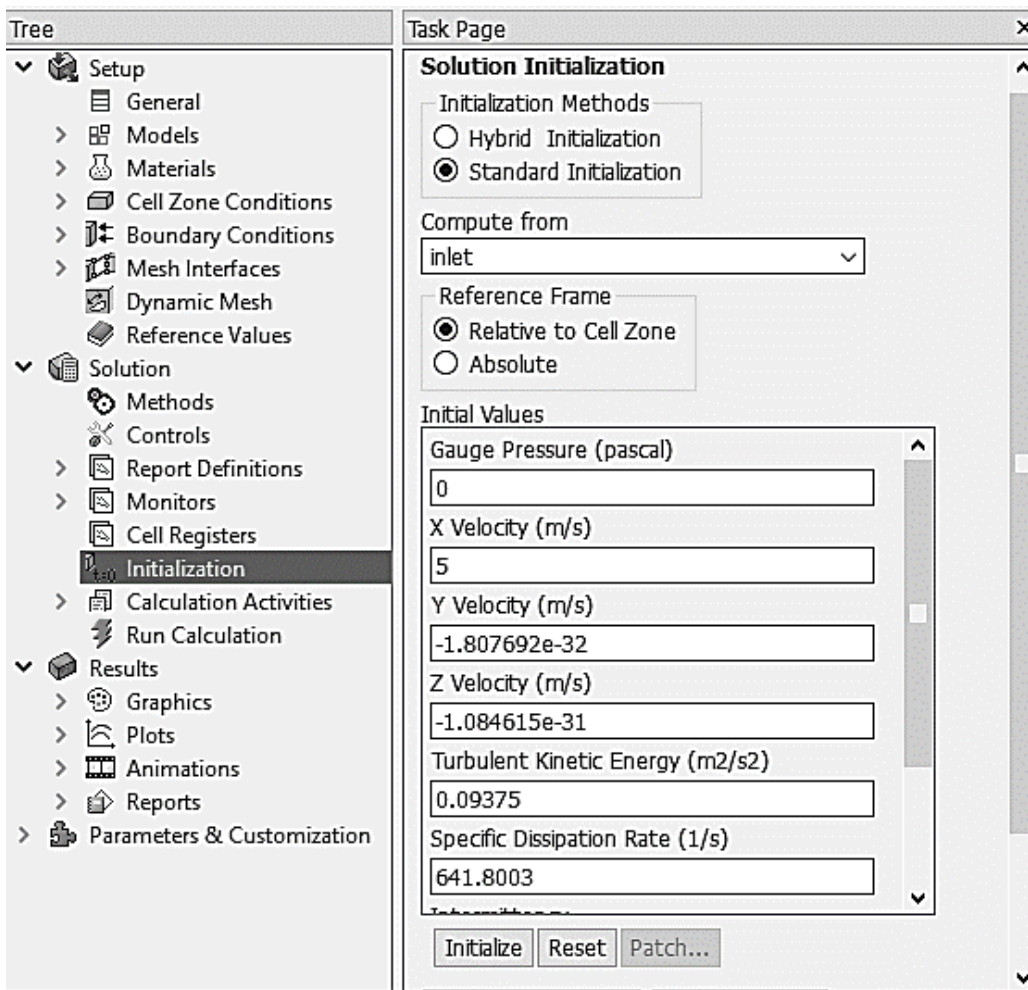
Figure D.17: Standard initialization
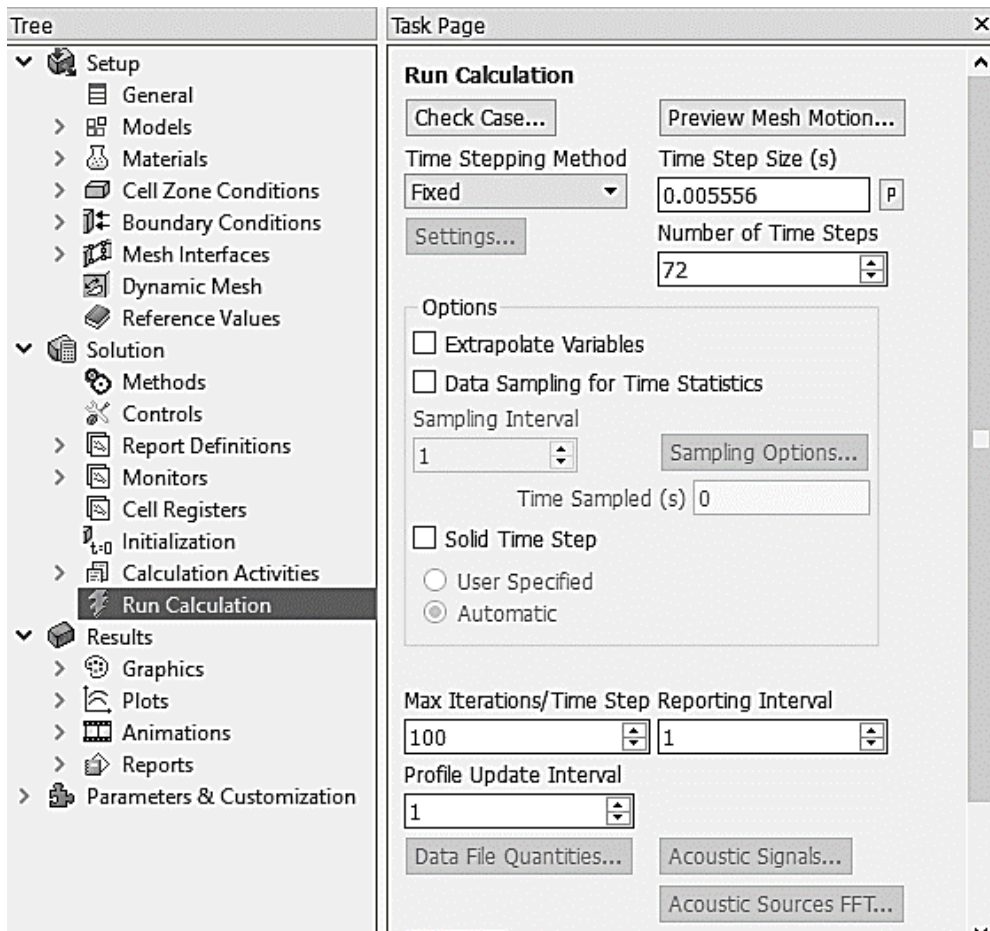
Figure D.18: Run calculation
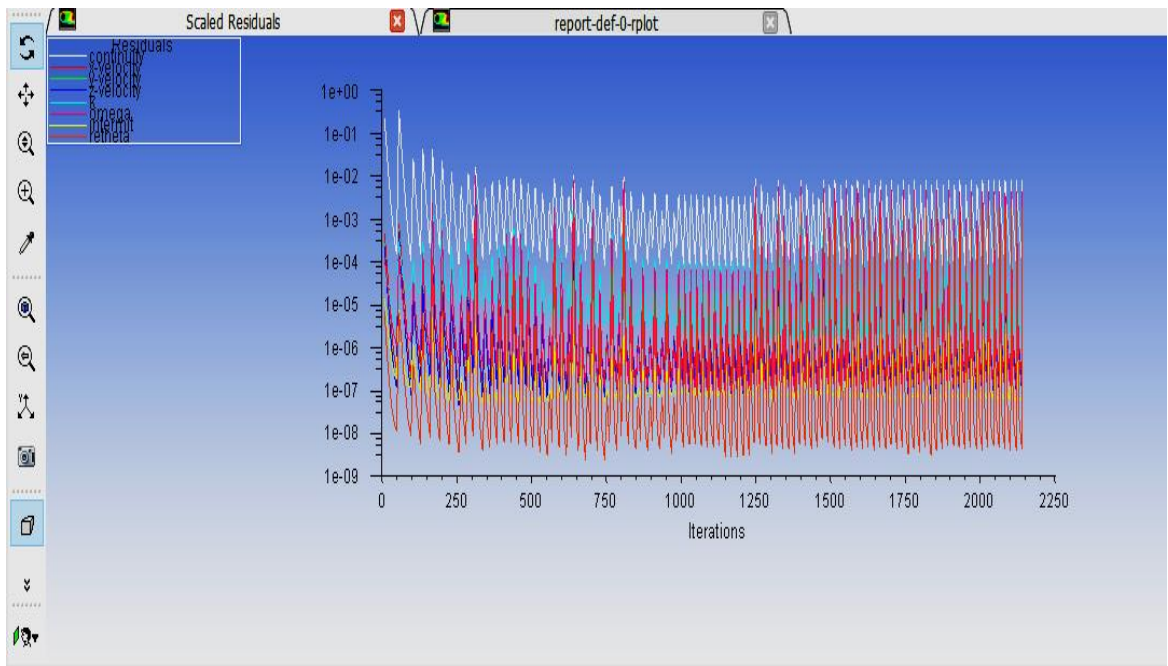
Fig D.19: Scaled residuals to achieve Convergence criteria throughout the study
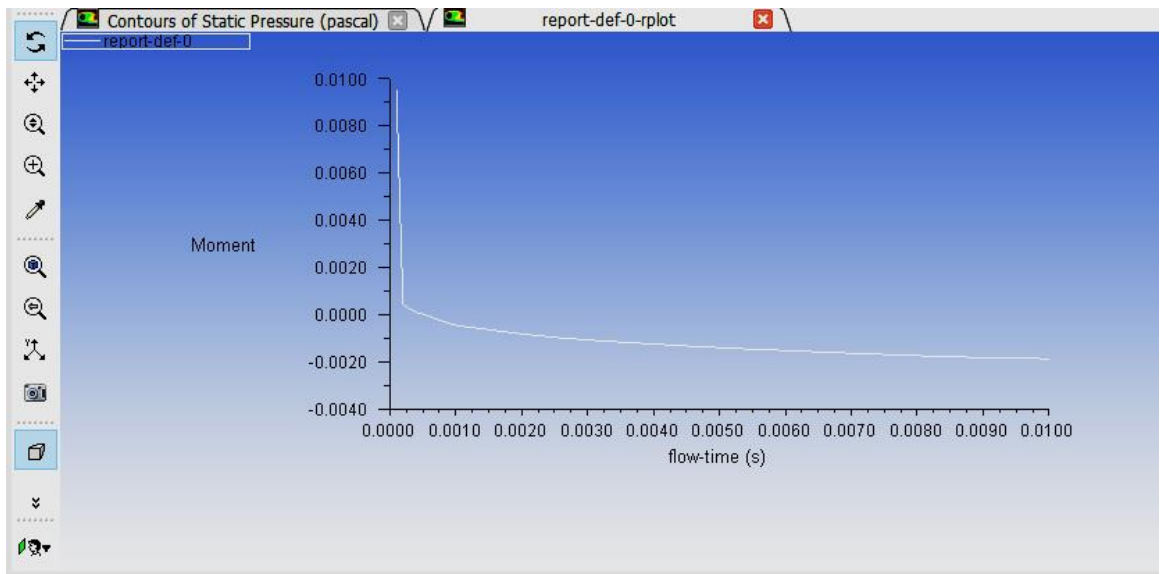
Fig D.20: Moment coefficient vs flow-time at 8 m/s
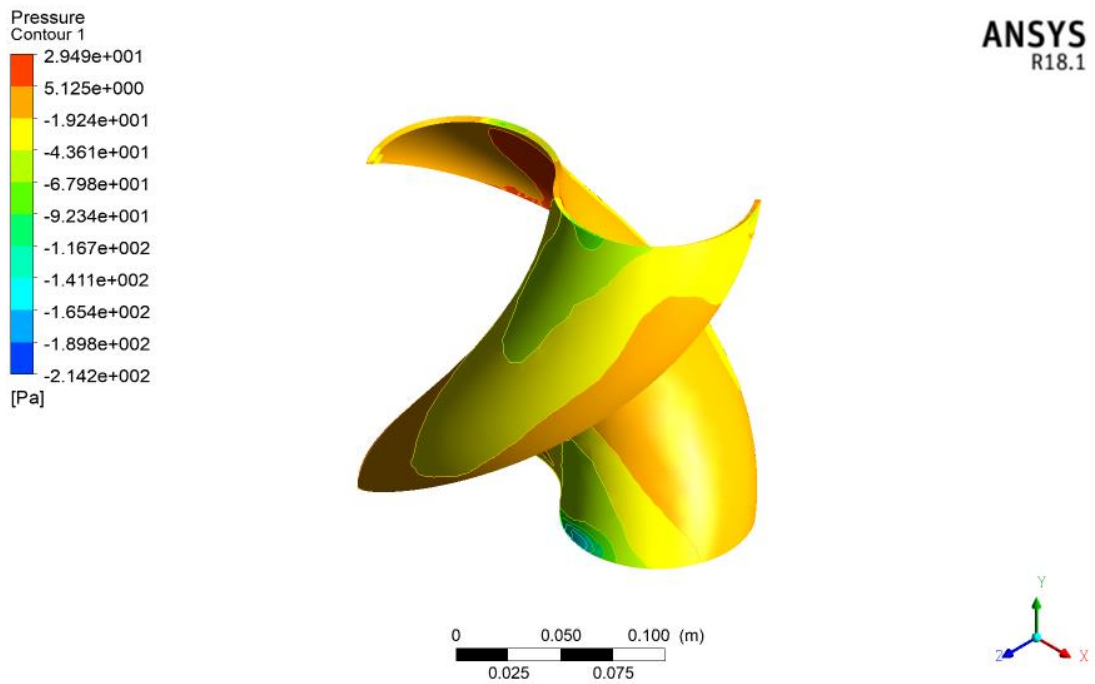
Fig D.21: Isometric view of Global pressure contours of the rotor at 5 m/s
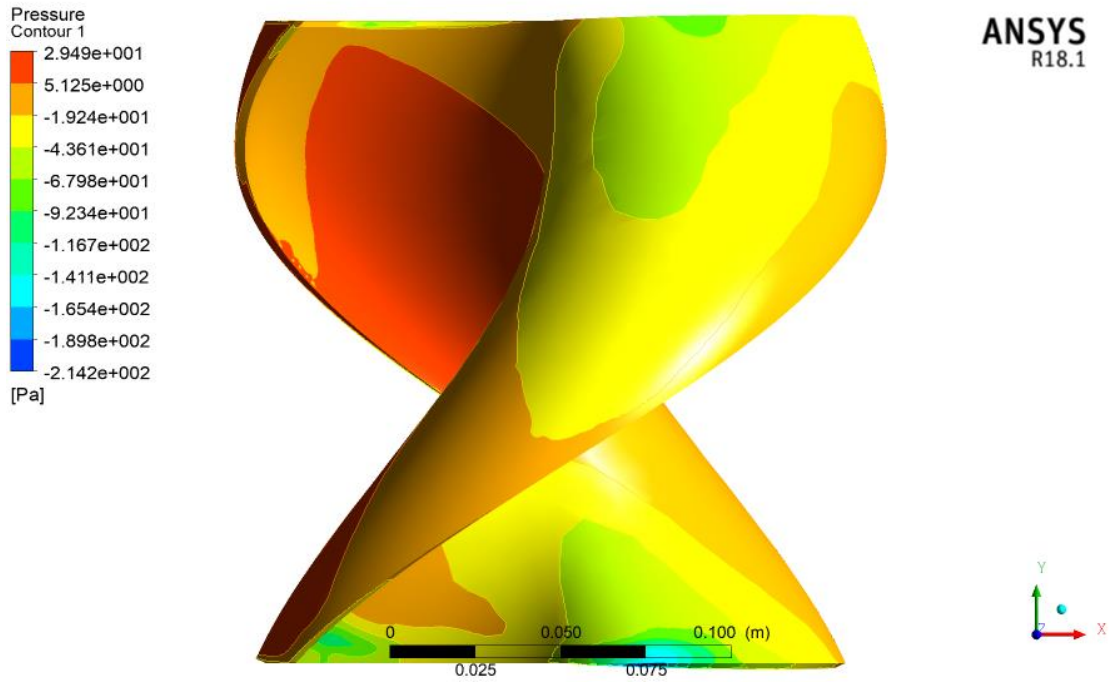
Fig D.22: Front view of Global pressure contours of the rotor at 5 m/s
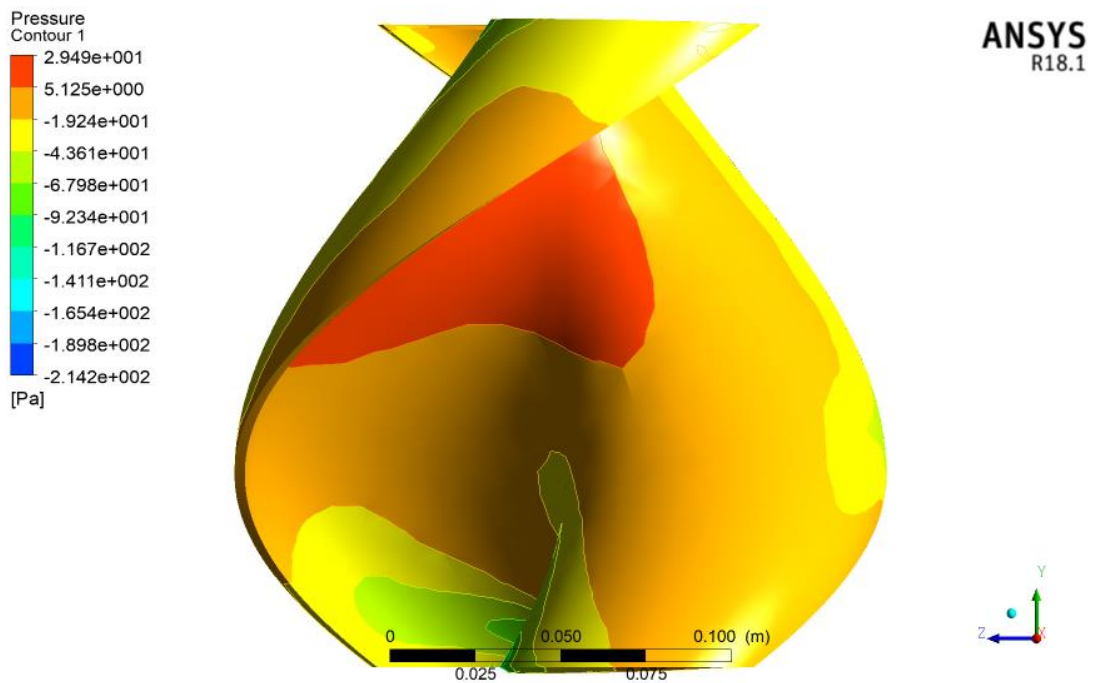
Fig D.23: Side view of Global pressure contours of the rotor at 5 m/s
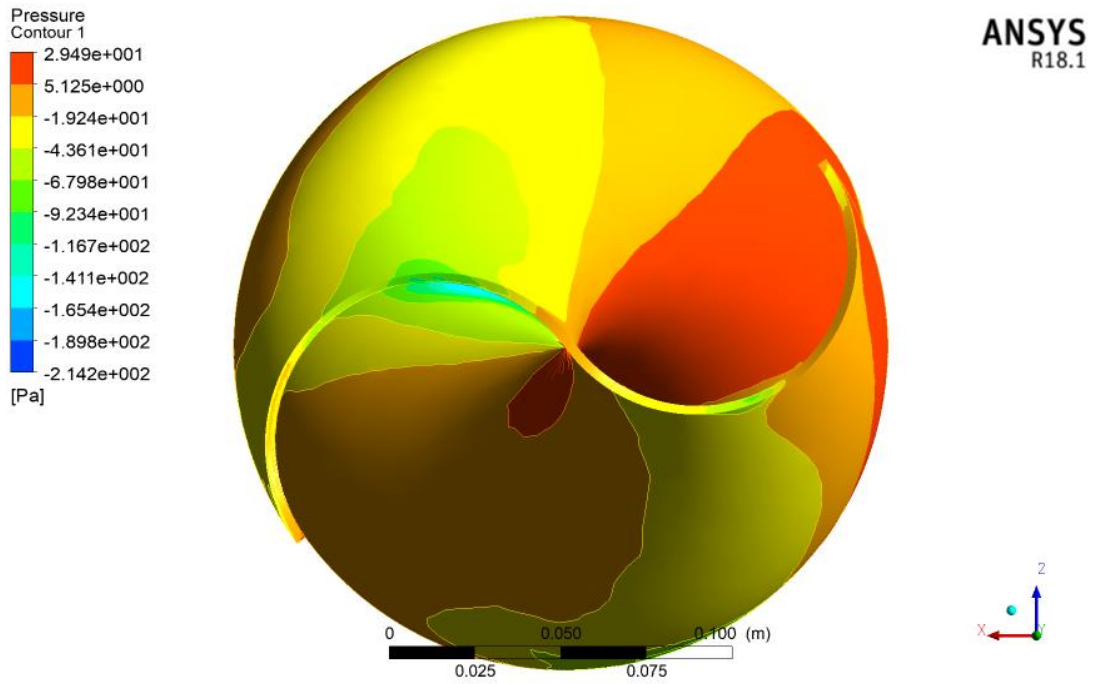
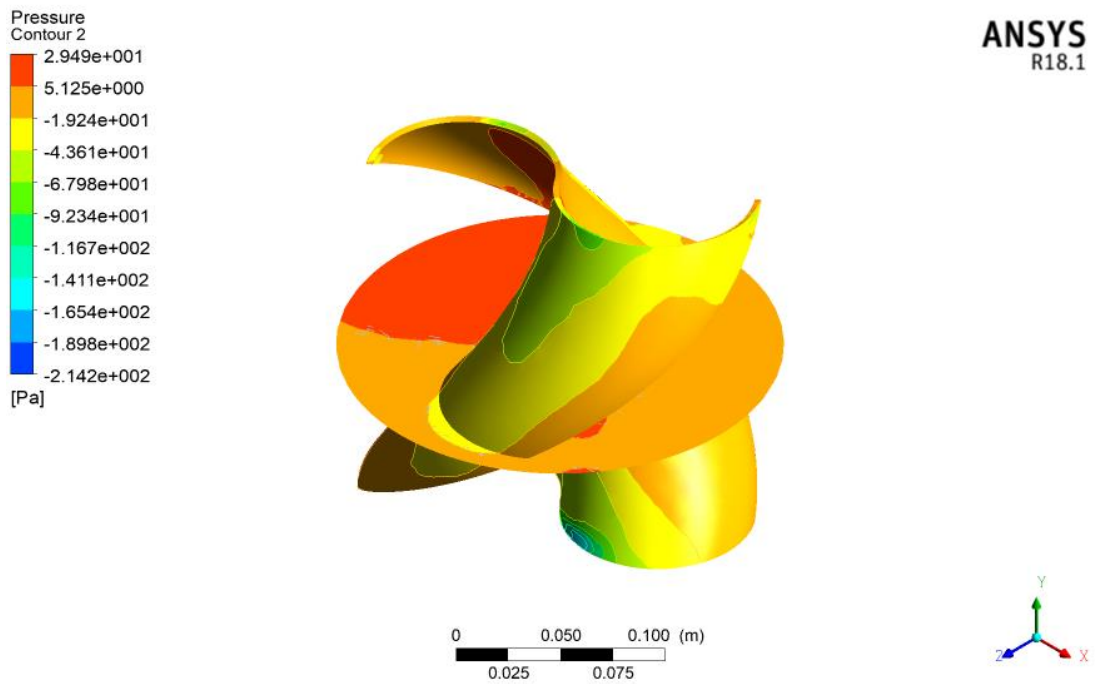Fig D.24: Top view of Global pressure contours of the rotor at 5 m/s

Fig D.25: Pressure contours of the rotor with mid-circular plane at 5 m/s

APPENDIX E: ORIGINALITY REPORT

Pradeep_Bartaula_III.pdf

| 9 | Submitted to University of Limerick
Student Paper | <1% |

| 10 | Submitted to Universiti Tenaga Nasional
Student Paper | <1% |

| 11 | Submitted to Kingston University
Student Paper | <1% |

| 12 | www.scirp.org
Internet Source | <1% |

| 13 | Submitted to Universiti Teknologi MARA
Student Paper | <1% |

| 14 | Submitted to University of Perpetual Help Sytem Laguna
Student Paper | <1% |

| 15 | studentsrepo.um.edu.my
Internet Source | <1% |

| 16 | Submitted to Higher Education Commission Pakistan
Student Paper | <1% |

| 17 | www.scribd.com
Internet Source | <1% |

| 18 | Ramesh K. Kavade, Pravin M. Ghanegaonkar. "Optimisation and performance analysis of vertical axis wind turbine with blade pitching at best position angle for different tip speed ratios", | <1% |